ORIGINAL PAPER

Innovative engine test bench set-up for testing of exhaust gas aftertreatment and detailed gas species analysis for CNG-SI-operation

Sebastian Tomin[1] · Kevin Keller[2] · Uwe Wagner[1] · Patrick Lott[2] · Thomas Koch[1] · Olaf Deutschmann[2]

Abstract

For an efficient reduction of methane slip, a precise understanding of exhaust gas after treatment under real conditions is essential. Since it is not possible to produce catalytic converters in near-series geometry on a laboratory scale, it is necessary to resort to significantly smaller sample catalysts. Therefore, an engine test bench was designed to ensure real operating conditions for such samples with the help of space velocity and temperature control. A comparison between the actual and reference values of the space velocity results in a small deviation of 0.1% on average. Furthermore, the pressure conditions at the catalyst have been measured showing a propagation of pressure oscillations from the engine outlet which in combination with the space velocity regulation show that real conditions could be applied to the catalyst sample. Subsequently, the exhaust gas concentrations were monitored with a Fourier transform infrared spectrometer. The catalyst material used is PdO on Al_2O_3, common for methane oxidation. The measurements show that the CH_4 conversion is higher under lean conditions, but is below complete conversion. In a final comparison between purely stoichiometric operation and dithering, the course of the CH_4 conversion rate over the test period is examined more closely. In addition to sampling pre- and post-catalyst, the exhaust gas composition is measured spatially resolved within a catalyst channel using special measurement technology. In the temporal course of the CH_4 emissions, a stabilizing effect due to the change of the operating mode can be seen, showing that dithering seems to prevent further deactivation.

Keywords Methane oxidation catalyst · Engine test bench · Exhaust gas aftertreatment · Spatial measurement · CH_4 · Lean gas engine · EGR

Abbreviations

AMA	Abgasmessanlage (exhaust gas measurement system)
CHP	Combined heat and power plant
COV	Coefficient of variation
CPSI	Cells per square inch
EGR	Exhaust gas recirculation
FTIR	Fourier-transform infrared
GC	Gas chromatograph
GHSV	Gas hourly space velocity
HCCI	Homogeneous charge compression ignition
IMEP	Indicated mean effective pressure
MFB50	50% Mass fraction burned
NGE	Natural gas engine
SCR	Selective catalytic reduction
URAS	Ultrarot-Absorptions-Schreiber (nondispersive infrared sensor)

✉ Sebastian Tomin
  sebastian.tomin@kit.edu

  Kevin Keller
  kevin.keller@kit.edu

  Uwe Wagner
  uwe.wagner@kit.edu

  Patrick Lott
  patrick.lott@kit.edu

  Thomas Koch
  thomas.a.koch@kit.edu

  Olaf Deutschmann
  deutschmann@kit.edu

1   Institute of Internal Combustion Engines (IFKM), Karlsruhe Institute of Technology (KIT), Kaiserstraße 12, 76131 Karlsruhe, Germany

2   Institute for Chemical Technology and Polymer Chemistry (ITCP), Karlsruhe Institute of Technology (KIT), Kaiserstraße 12, 76131 Karlsruhe, Germany

1 Introduction

Due to their lower carbon dioxide (CO_2) and pollutant emissions and their partly higher efficiency compared to diesel engines, natural gas engines (NGEs) are primarily used in maritime and stationary applications. There they are often operated as lean-burn engines. Despite the currently strained supply situation particularly in Europe [40], natural gas with its main component methane (CH_4) will remain indispensable for a reliable energy supply and as a fuel in the coming years. In addition to conventional fossil sources, also sustainable biogas and sludge gas or methane from power-to-gas processes that allow to store excess energy from renewables such as wind and solar in chemical energy carriers will gain importance in the foreseeable future. Despite the overall low pollutant levels emitted from lean-burn NGEs, methane slip as a result of incomplete combustion leads, if left untreated, to methane emissions, which have a considerable impact on climate change due to the more than 20 times higher global warming potential compared to CO_2 [35]. Possible engine sources of incompletely burnt methane result from the combustion chamber geometry or the engine design as well as from the operating strategy. For example, the greater the valve overlap (engine design), the more unburnt methane can escape directly. With regard to combustion chamber design, flame quenching plays a significant role. In crevices where the surface/volume ratio is very high, the flame front does not reach the fuel–air mixture due to the high heat dissipation. This is especially the case in the topland above the piston rings and is therefore virtually unaffected by the operating strategy. Another influence on flame quenching (especially near the cold combustion chamber walls) originates from the charge movement and the associated turbulence. With a higher degree of turbulence, the flame can advance closer to the combustion chamber walls and more methane can be oxidized. Other causes of quenching, on the contrary, can be influenced more by a change in the operating parameters. For example, the fuel–air mixture, the pressure and the temperature play a major role in the stability of combustion. A lean fuel–air mixture, for example, increases the risk of locally too lean zones due to inhomogeneities, as a result of which combustion can no longer be maintained and emissions of unburnt methane increase [12, 41, 50, 66, 69, 75].

In addition, further tightening of emissions legislation is expected, which could bring methane emissions even further into focus. Consequently, questions regarding exhaust gas aftertreatment will remain relevant [49]. Following a retrofit idea, the operating strategy should be optimized in terms of emissions while avoiding major physical modifications to the engine. The influence of the combustion chamber geometry on methane slip can only be dealt with to a limited degree by adjusting the operating strategy. Therefore, an exhaust gas aftertreatment system is required. Consequently, optimization of engine operation aims at positively influencing the conditions at the catalytic converter as well as the raw emissions of the untreated pollutants [69].

Under lean conditions, CH_4 is most efficiently converted over catalysts based on palladium (Pd) [14, 23, 69], most likely via a Mars–van Krevelen mechanism taking place over the active species PdO [36, 47, 64, 69, 74] that is commonly supported on metal oxides such as alumina (Al_2O_3). Despite their initially high activity, Pd catalysts suffer from severe inhibition by the inevitable exhaust component water (H_2O), which was attributed to an accumulation of hydroxyl groups on the catalyst surface that particularly block the active PdO particles [3, 29, 57, 69, 72]. In addition, catalyst deactivation may take place at elevated temperatures [16, 38, 69], e.g. due to noble metal particle sintering [30, 69].

In real exhausts, not only steam but also pollutants such as carbon monoxide (CO), formaldehyde (CH_2O) and nitrogen oxides (NO_x) interact with the catalyst, and sulphur-containing compounds such as hydrogen sulphide (H_2S) or sulphur oxides (SO_x) can act as a strong catalyst poison [49, 69]. In this respect, optimized catalyst formulations can ensure high activity and stability. For instance, bimetallic Pd–Pt catalysts were suggested to mitigate water inhibition [11, 42], reduce sintering [55] and slightly improve the performance in the presence of sulphur species [24, 27]. Moreover, using ceria (CeO_2), zirconia (ZrO_2) or tin oxide (SnO_2) as a support material was reported to reduce the negative impact of water [15, 39, 43, 54].

However, choosing appropriate engine operation strategies can significantly contribute to maintaining high pollutant conversion rates as well. For instance, high-frequency lean-rich cycling, the so-called dithering, can increase pollutant conversion particularly in the low-temperature regime—a concept that is known for stoichiometric applications since decades [32, 53, 69] and that currently enjoys growing popularity again [17, 34, 60, 69]. In a comparable way, periodic cycling between lean and short rich conditions can enhance the CH_4 oxidation performance of Pd catalysts operated under lean conditions in humid exhaust environments by decomposing adsorbed hydroxyl species during the substoichiometric phase along with an optimization of the morphology and oxidation state of the noble metal particles [9, 21, 22, 37, 69]. Furthermore, rich pulses were demonstrated to decompose sulphur species that are adsorbed on Pd–Pt methane oxidation catalysts, hereby enabling efficient regeneration of harshly aged catalysts [47, 48]. Notably, the transfer of such catalyst operation strategies to real-world applications is possible [27, 44]. Lehtoranta et al. have investigated regeneration under stoichiometric conditions with sulphur-poisoned methane oxidation catalysts and real engine exhaust gas. They found that with this form of reactivation, positive results were achieved after just

a few minutes [44]. So, additionally to conventional regeneration under stoichiometric conditions, dithering could have a beneficial impact since it could improve the catalytic activity itself during the reactivation and promote the regeneration effect due to the rich pulses occurring in dithering mode.

To investigate the influence of real exhaust gas on the catalyst performance, it is important to examine different catalyst samples. However, since the coating of a monolith with a near-series geometry is difficult to realize on a laboratory scale and is uneconomical, a test bench concept is needed that bridges the gap between real application and laboratory. For this reason, the present study aims at developing a set-up that integrates catalyst samples into an engine test bench and ensures the most realistic possible conditions with regard to temperature, pressure and space velocity. In addition, a direct coupling of such an engine test bench with advanced catalyst testing technologies is key to understand how catalysts behave under challenging real-world conditions. Therefore, a natural gas engine is coupled with an on-line effluent gas analysis by means of a Fourier transform infrared (FTIR) spectrometer that monitors either engine-out raw emissions or the activity of a monolithic catalyst sample during realistic load control of the engine. An external sample loop was set up that allows to measure spatially resolved species concentration profiles within a single channel of the catalytic converter. Inspired by spatial profiling techniques well known at lab scale [18, 46, 61], the novel setup presented herein provides direct insights into inhibition and deactivation phenomena taking place in real-world exhaust gases. Therefore, different engine operation modes, i.e. lean, stoichiometric and dithering, are applied and their impact on a PdO/Al_2O_3 methane oxidation catalyst is studied by means of end-of-pipe gas phase analysis as well as spatial profiling. In the following, it will be shown how well real conditions can be represented on laboratory samples and what findings can be gained using corresponding measurement technology under typical engine operating conditions.

2 Experimental methods

2.1 Experimental set-up

2.1.1 Test engine

Table 1 shows the data of the base engine, which is a 2.2 l 3-cylinder engine (Table 1) used in industrial applications. It is operated stoichiometrically without turbocharging and exhaust gas recirculation (EGR). Since gas engines, which often rely on EGR to reduce engine-out nitrogen oxides emissions [65] or lean operation, are used in many applications, appropriate modifications to the basic engine are necessary to be able to examine catalytic converters under

Table 1 Data of base engine

Properties	Values
No. of cylinders	3
Bore/stroke (mm)	92/110
Displacement (l)	2,19
Max. nominal speed (min^{-1} ǀ rpm)	2200–2800
Power (kW)	42
At speed (min^{-1} ǀ rpm)	2800
Max. torque (Nm)	160
At speed (min^{-1} ǀ rpm)	1300–1600
Minimum idling speed (min^{-1} ǀ rpm)	900
Operating conditions	Stoichiometric
Charging	Naturally aspirated

real conditions more closely. Pure lean-burn would already be possible with the standard engine, but would lead to a loss of power due to the lack of turbocharging, which would mean that only operating points with low loads could be represented. For this reason, an external boost pressure supply is used, which in combination with a backpressure valve simulates a turbocharger (Figs. 1 and 2). In addition, the intake manifold was replaced by a proprietary design that enables the recirculation of exhaust gas and, for future investigations, accommodates six injectors for the injection of species such as methanol or water (as a further measure for nitrogen oxide reduction).

The fuel is added to the air via a mixer and a pressure-regulating valve. The mass flows of both media are measured by means of Coriolis scales (s. Figure 2 and Appendix). In the case of natural gas, also the gas composition is determined with the aid of a gas chromatograph (GC, ABB Totalflow). The exhaust gas for the EGR is taken upstream of the back-pressure valve and routed to the intake manifold via an EGR cooler. The rate is determined by comparing the CO_2 content in the intake manifold with that in the raw exhaust gas with the help of a nondispersive infrared sensor (Ultrarot-Absorptions-Schreiber (URAS), ABB Uras26) (Appendix).

2.1.2 Exhaust gas system

2.1.2.1 Regulation strategies A turbocharger generates a backpressure in the exhaust gas via its flow resistance which can be adjusted to a target pressure differential to the intake manifold pressure by means of a backpressure valve. The EGR rate is directly controlled via an EGR valve. In addition, the exhaust system is equipped with an FTIR spectrometer as well as an exhaust gas measurement system (AMA, AVL AMA 4000) to measure the exhaust gas composition both up and downstream the catalytic converter (Fig. 2).

Fig. 1 Principle sketch of a turbocharged CNG engine using EGR
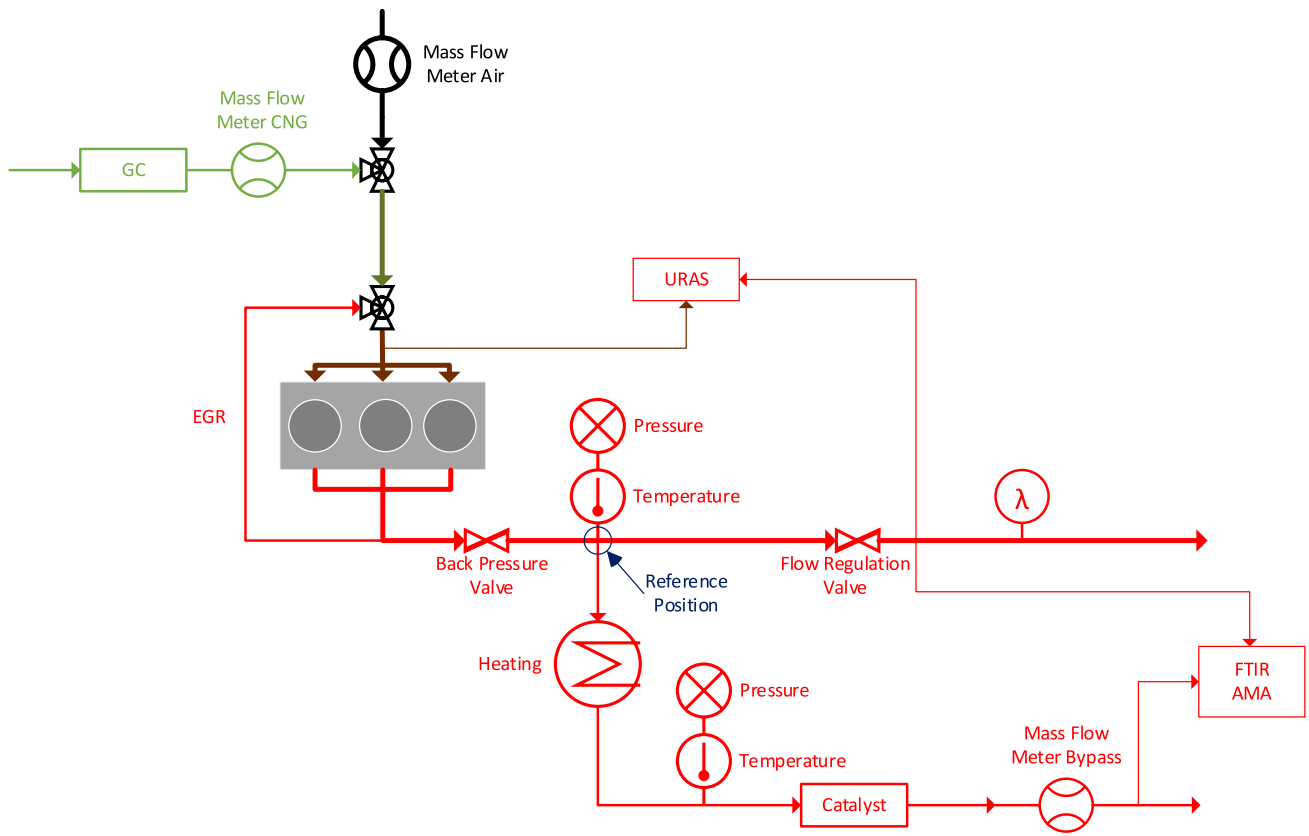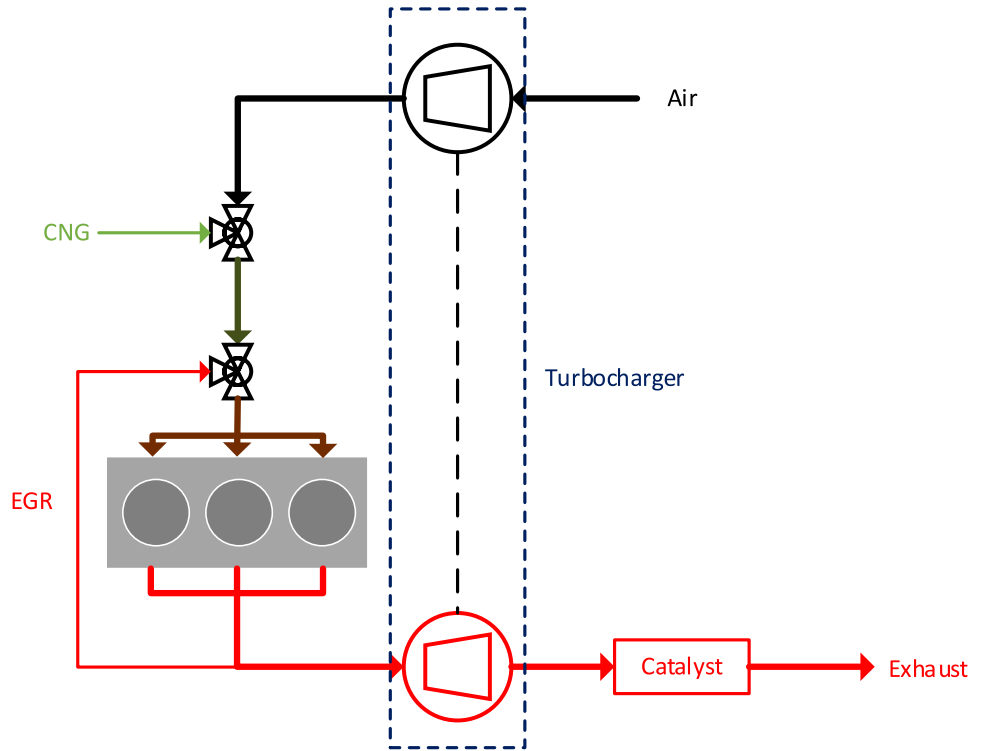

Fig. 2 Principle sketch of the engine test bench set-up [68]

An important parameter in exhaust gas catalysis for comparing different catalyst formulations and geometries is the gas hourly space velocity (GHSV). It is defined as the ratio between the volume flow rate through the catalyst $\dot{V}_{cat}$ and the catalyst volume (monolith) V_{cat}:

$$\text{GHSV} = \frac{\dot{V}_{cat}}{V_{cat}} \tag{1}$$

The volume results from the geometry (diameter d_{cat} and length l_{cat} of the monolith), and the volume flow is the ratio between mass flow $\dot{m}_{cat}$ and density ρ_{exh}. Since the assumption of ideal gas behaviour is permissible under the conditions in an exhaust system for internal combustion engines, the density can be determined using the following ideal gas equation:

$$\text{GHSV} = \frac{\frac{\dot{m}_{cat}}{\rho_{exh}}}{V_{cat}} = \frac{\dot{m}_{cat} \cdot \frac{R \cdot T_{cat}}{p_{cat} \cdot M_{exh}}}{\pi \cdot \frac{d_{cat}^2}{4} \cdot l_{cat}} \tag{2}$$

In Eq. (2), the geometric quantities are given by the catalytic converter and are therefore known. Furthermore, the molar mass of the mixture (M_{exh}) can be determined by measuring the exhaust gas composition. If the temperature (T_{cat}), pressure (p_{cat}) and mass flow ($\dot{m}_{cat}$) are also measured, the space velocity can be calculated with the universal gas constant R. Two control modes can be selected in the test bench set-up: It is possible to either specify a target space velocity directly or to control to a 'reference' GHSV. The reference position results from the typical installation position of a series catalytic converter in turbo-charged engines. In these applications, a catalytic converter is often installed after the turbocharger turbine (Fig. 1) and thus after the backpressure valve in the test bench set-up (Fig. 2). To ensure that the temperature at the catalyst sample is the same as at the reference point, a heating tape is used together with the associated temperature control. The exhaust gas composition at both locations is also the same. The pressure at both the reference and the sample is measured using pressure sensors. Now the geometric variables and the mass flow are missing for the complete definition of the reference. Due to the retrofit idea, the volume of the series catalytic converter of the base engine is chosen as the reference volume. Under real conditions, the entire exhaust gas mass flow (corresponding to the sum of all mass flows entering the engine combustion chamber, namely mass flow of intake air $\dot{m}_{air}$ and mass flow of CNG $\dot{m}_{CNG}$) would also flow through the catalytic converter. This results in the following Eq. (3) for the reference mass flow:

$$\dot{m}_{ref} = \dot{m}_{air} + \dot{m}_{CNG} \tag{3}$$

The actual value of the GHSV control is the value at the catalyst sample. The geometry is given by the dimensions of the catalyst sample, and the mass flow through the sample (bypass) is measured with the help of a mass flow metre from Systec Controls, type DF8. If automatic control to the reference is required, the space velocity at the reference position is set in the control system, which in turn adjusts the flow regulation valve and thus the actual value accordingly. With both control modes, it is therefore possible to examine the catalytic converter performance both under the premise of a retrofit and with the motivation of finding an optimal catalytic converter volume [68]. The corresponding measurement devices are listed in the Appendix.

2.1.2.2 Catalyst probe The GHSV plays a decisive role for the investigation of exhaust gas catalysts. The bypass concept allows using catalyst samples with significantly smaller volumes than those of full-scale serial converters. Notably, smaller substrates are easier to coat (especially on a laboratory scale) and require less material. In addition, smaller geometries facilitate the coating of more complex novel monolithic structures, for instance as produced by 3D printing processes. In this study, the sample was produced using the dip-coating procedure. For this, a slurry containing the 2 wt. % PdO/Al$_2$O$_3$ was coated on to the cordierite monolith until the desired noble metal loading of 80 g/ft3 was achieved. The received sample (length 5 cm, diameter 2.54 cm, c.f. Table 2) can be integrated into the exhaust duct with the aid of a sample holder (Fig. 3). The sample holder is a stainless-steel lantern modified with regard to glass tube and sealing material for the use at exhaust gas temperatures. This ensures an optical access to the area in front and behind of the monolith, which is a prerequisite for aligning the capillary-based sampling technique exploited for spatial profiling (SpaciPro, Chapter 3). The sample holder is mounted into the bypass at both ends by means of flanges and clamps that are gas-tight during operation, but which can be easily loosened and tightened for fast exchange of the catalyst sample.

Table 2 Properties of the used catalyst probe

Properties	Values
Catalyst material	2 wt% PdO/Al$_2$O$_3$
Loading	80 g/ft3
Monolith material	Cordierite
Length	5 cm
Diameter	2.54 cm
Cell density	600 CPSI

Fig. 3 Left: Sample holder for integration of catalyst samples into exhaust tailpipe. Right: Catalyst sample within sample holder

Table 3 Test matrix

Measuring point	Measuring position reg. cat	Ignition timing	λ	EGR	GHSV
				%	1/h
1	Before	Early	1.4	0	167,000
	After	Early	1.4	0	166,000
2	Before	Early	1.4	0	170,000
	After	Early	1.4	0	170,000
3	Before	Late	1.4	0	173,000
	After	Late	1.4	0	172,000
4	Before	Early	1	0	151,000
	After	Early	1	0	147,000
5	Before	Late	1	0	155,000
	After	Late	1	0	154,000
6	Before	Late	1	10	139,000
	After	Late	1	10	138,000

2.2 Experimental procedure

The experiments in this study focus on two different operating ranges of a gas engine that are particularly relevant for maritime applications or combined heat and power plants (CHPs). First, 'normal' operation under lean conditions is realized; second, engine operation parameters are chosen that allow to (re-)activate methane oxidation catalysts, namely rich conditions or rich pulses. For this reason, the dithering mode of the engine control unit is used to generate a Lambda oscillation of $\pm 5\%$, which results in periodic deviations into rich operating ranges. Since gas engines are often operated with EGR in the above-mentioned applications, measurements are also carried out at an EGR rate of 10%.

These tests aim at demonstrating the capabilities of the test bench set-up, i.e. operation of a lab-scale catalyst sample under various real-world operation conditions. In addition to the detailed analysis of the exhaust gas composition, the measurements also focus on the pressure conditions present at the catalyst sample. For this purpose, fast low-pressure indication (Appendix) is used both up- and downstream of

the sample. These data can serve as input parameters for simulative investigations on the heterogeneous (phase of catalyst differs from that of reactants or products) catalyst during future studies.

The tests were conducted using the reference GHSV regulation mode. Table 3 summarizes the test matrix with the varied input variables. The tests were carried out at a load of ~ 9 bar indicated mean effective pressure (IMEP) and a speed of 1500 1/min (typical speed for CHP applications). The Fourier-transform infrared (FTIR) spectrometer enables the simultaneous analysis of a significantly higher number of different exhaust gas species compared to a conventional exhaust gas analyser. In the following, concentrations of NO, NO_2, N_2O, NH_3, CO, CH_4 and SO_2 and their dependency on engine operating conditions will be discussed. The temperature before and after the catalyst sample, referred to as $T_{upstream}$ and $T_{downstream}$, respectively, were measured by means of type K thermocouples placed approx. 30 mm up- and downstream of the sample.

3 Results and discussion

3.1 Influence of air–fuel ratio

In addition to the exhaust gas species, Table 4 also shows the GHSV and the temperatures up- and downstream of the catalyst. Since the air mass flow must be increased at constant load compared to stoichiometric operation, the GHSV is higher for lean operation points. The temperature shows the influence of both lean combustion and ignition timing. As a result of the changed heat capacity of the cylinder charge due to dilution, the temperatures are lower than those in purely stoichiometric operation without EGR. The ignition timing leads to an increase in exhaust gas temperature with late adjustment, as the efficiency deteriorates and thus more energy remains unused in the final gas. An important point for assessing the emission measurements is the lambda control, especially in stoichiometric operation. Figure 4 shows the measured course of lambda over the crank angle. It clearly shows the lambda deviations of $\pm 5\%$. The influence of various parameters of the lambda oscillation (frequency,

Table 4 Test matrix with results except for the hydrocarbons

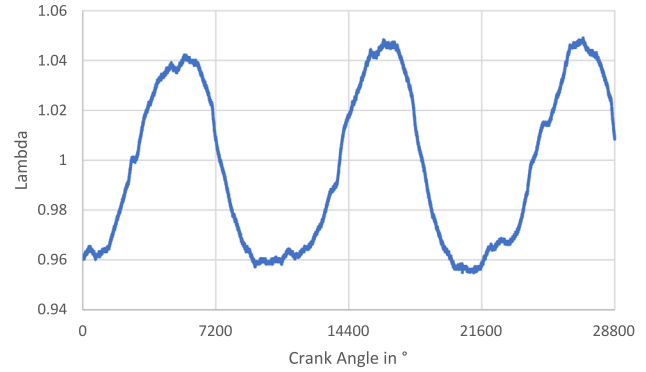| Measuring point	Measuring position reg. cat	Ignition timing	λ	EGR %	GHSV 1/h	$T_{upstream}$ Cat °C	$T_{downstream}$ Cat °C	NO ppm	ΔNO %	NO_2 ppm	$ΔNO_2$ %	N_2O ppm	$ΔN_2O$ %	CO ppm	ΔCO %	CH_4 ppm	$ΔCH_4$ %	NH_3 ppm	$ΔNH_3$ %	CO_2 %	$ΔCO_2$ %	SO_2 ppm	$ΔSO_2$ %	H_2O %	$ΔH_2O$ %	O_2 %	$ΔO_2$ %
1	Before	Early	1.4	0	167,000	546	534	1950	5	79	−24	1	−45	352	100	931	80	0	0	7.0	−1	0	−172	13.2	−5	6.6	3
	After	Early	1.4	0	166,000	545	533	1846		98		1		1		183		0		7.1		1		14.0		6.4	
2	Before	Early	1.4	0	170,000	552	538	1104	−5	78	22	0	−70	352	100	882	81	0	0	7.1	−1	0	−498	12.1	−15	6.7	4
	After	Early	1.4	0	170,000	553	538	1158		61		1		1		168		0		7.1		1		13.9		6.4	
3	Before	Late	1.4	0	173,000	576	556	540	−12	72	56	0	−39	332	100	734	82	0	0	6.8	−5	0	−165	17.3	19	6.7	3
	After	Late	1.4	0	172,000	575	555	607		31		0		1		133		0		7.1		1		14.0		6.5	
4	Before	Early	1	0	151,000	632	590	2688	54	5	−442	1	−629	5007	76	712	67	0	−148,083	9.0	−2	2	−98	18.3	0	0.7	55
	After	Early	1	0	147,000	628	588	1239		25		5		1215		236		685		9.2		4		18.3		0.3	
5	Before	Late	1	0	155,000	665	611	2241	56	4	−289	1	−433	5315	73	616	75	1	−126,681	9.0	−3	2	−109	18.4	−1	0.7	53
	After	Late	1	0	154,000	661	611	980		16		3		1460		155		643		9.2		4		18.5		0.3	
6	Before	Late	1	10	139,000	617	569	1714	54	5	−232	1	−371	4657	73	815	67	0	−94,468	9.0	−2	1	−168	18.3	0	0.7	45
	After	Late	1	10	138,000	620	573	787		18		2		1235		272		448		9.3		4		18.3		0.4	

Fig. 4 Lambda plotted against crank angle at stoichiometric conditions

Table 5 Values of Lambda swing

Equivalence air–fuel ratio (λ)	
Mean value	1
Amplitude	0.05
Frequency	0.85 Hz

Table 6 Gas composition of used CNG

Species	Formula	Unit	Value
Methane	CH_4	vol-%	91.23
Ethane	C_2H_6	vol-%	4.75
Propane	C_3H_8	vol-%	1.13
Isobutane	i-C_4H_{10}	vol-%	0.198
Butane	n-C_4H_{10}	vol-%	0.188
Pentane	n-C_5H_{12}	vol-%	0.042
Isopentane	i-C_5H_{12}	vol-%	0.031
Hexane	C_6H_{14}	vol-%	0.007
Carbon dioxide	CO_2	vol-%	1.29
Nitrogen	N_2	vol-%	1.14
Methane number	–	–	79.7
Calorific value	H_S	kWh/m^3	11.504
Heating value	H_i	kWh/m^3	10.390
Standard density	$\rho_{Standard}$	kg/m^3	0.7934
Upper Wobbe index	W_S	kWh/m^3	14.686

amplitude and mean value in Table 5) was investigated especially for gas engines in [63].

3.1.1 CNG composition

The natural gas used for the experiments originates from the Karlsruhe city grid. To determine the composition, a gas chromatograph (GC) was used to analyse the concentrations of certain species in the natural gas. In this case, the natural gas consists of almost 94% methane and also

contains relevant proportions of ethane (~ 4%), propane and butane. (Table 6). In addition, the natural gas can also contain components that cannot be detected but which may impact the catalyst, such as sulphur. The fuel composition has an influence not only on the catalyst but also on the combustion process itself, which is why the methane number and the calorific values are calculated with the help of the measured concentrations.

3.1.2 Pressure conditions

Figure 5 shows the pressure curves at various points in the exhaust system over a working cycle. The top curve shows the pressure directly after the engine, and the other two the pressures up- and downstream of the catalytic converter. Three deflections can be seen in all curves. These result from the gas exchange of the individual cylinders. The pulsations are (attenuated) passed on to the catalyst sample. The higher mean value for the pressure after the engine comes from the exhaust backpressure control. A minimal difference in the mean value of the two curves at the catalytic converter is also noticeable. This can be attributed to the flow resistance of the catalyst sample. An evaluation of the maxima, which occur with a time lag from one another, would provide information about the duration of the flow from position to position.

3.1.3 Gas hourly space velocity (GHSV)

A decisive factor for a reliable and efficient performance of tests in the context of exhaust gas aftertreatment is the adjustment of the test conditions. In catalysis, these are strongly influenced by the space velocity. In fluctuating

operation, as is the case on an engine test bench (Fig. 5), manual adjustment would be very difficult and would require considerable effort, hence in this case a control concept (Chapter 2.2) must be developed. Since, as explained in Chapter 2.1.2, many fluctuating measured variables are necessary for calculating the GHSV, there are quickly occurring and changing deviations to which a PID controller reacts sensitively, making the adjustment of the individual control components essential. After adjusting the control parameters, there is a deviation between the setpoint and actual value of on average approx. $\pm 0.1\%$ (Table 7).

Table 7 Values of GHSV at the catalyst probe, at the reference position and their deviation

GHSV catalyst 1/h	GHSV reference 1/h	Deviation %
166,519.1	166,551.7	0.0
165,823.5	166,955.9	− 0.7
169,601.1	168,425.6	0.7
169,776.7	169,604.6	0.1
173,223.3	174,036.9	− 0.5
171,597.2	174,967.6	− 1.9
150,684.9	150,569.2	0.1
147,368.1	148,414.9	− 0.7
155,167.2	156,421.2	− 0.8
153,563.4	154,170.6	− 0.4
139,369	138,079.4	0.9
137,865.4	137,294.2	0.4
Mean value in %		− 0.1

Fig. 5 Pressure oscillations in the exhaust
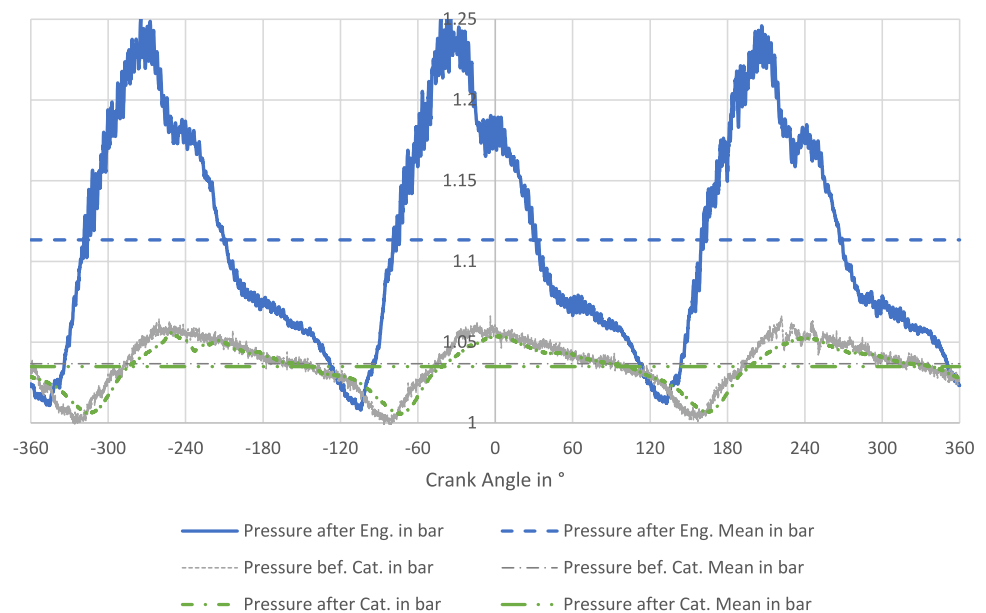
3.1.4 Exhaust gas species

In the following, the results of the concentration measurements conducted for all operation points listed in Table 3 are examined in more detail, broken down by the individual species or species groups.

Table 8 Diagrams of the most relevant species emissions and temperatures as function of 50% mass fraction burned (MFB50)
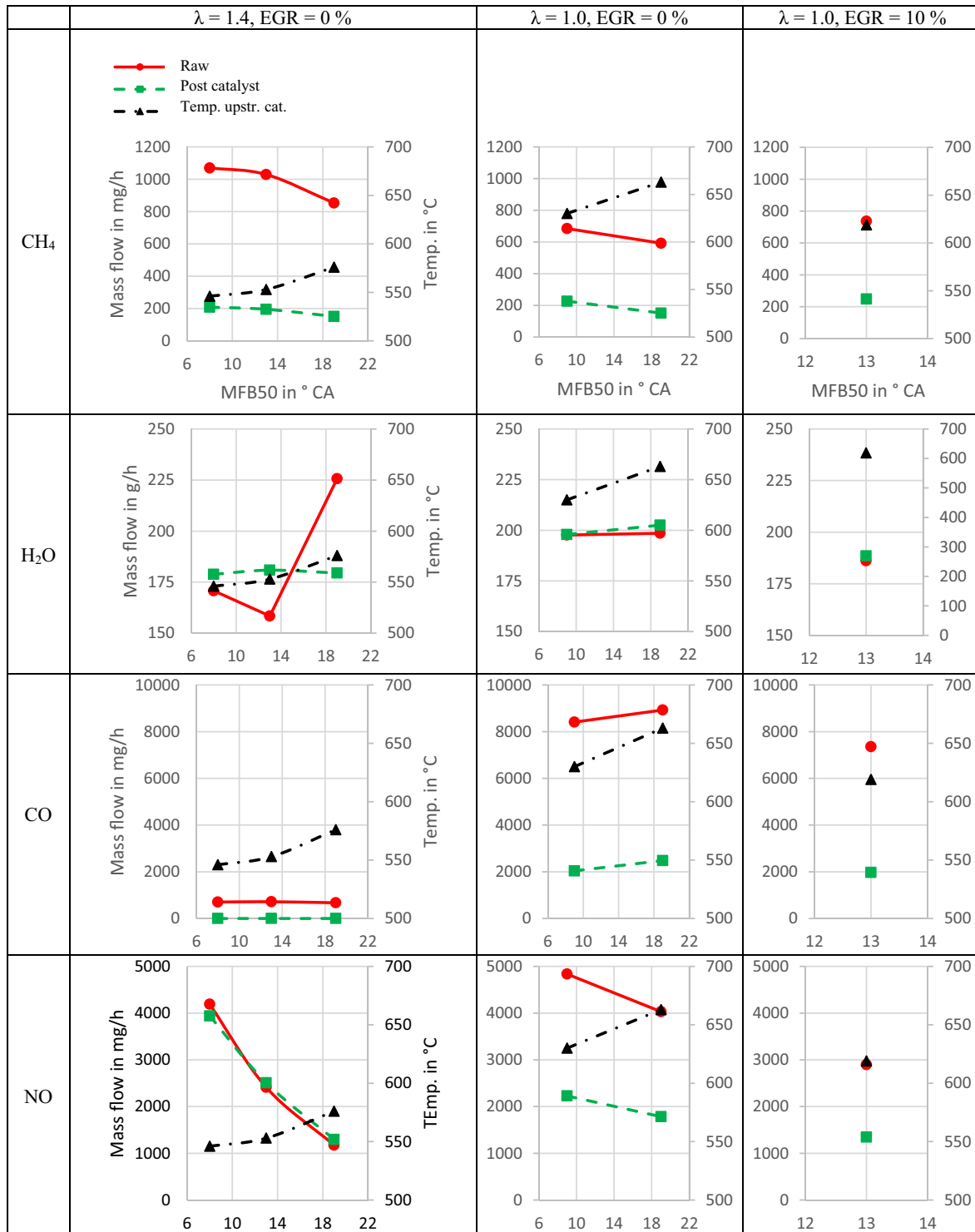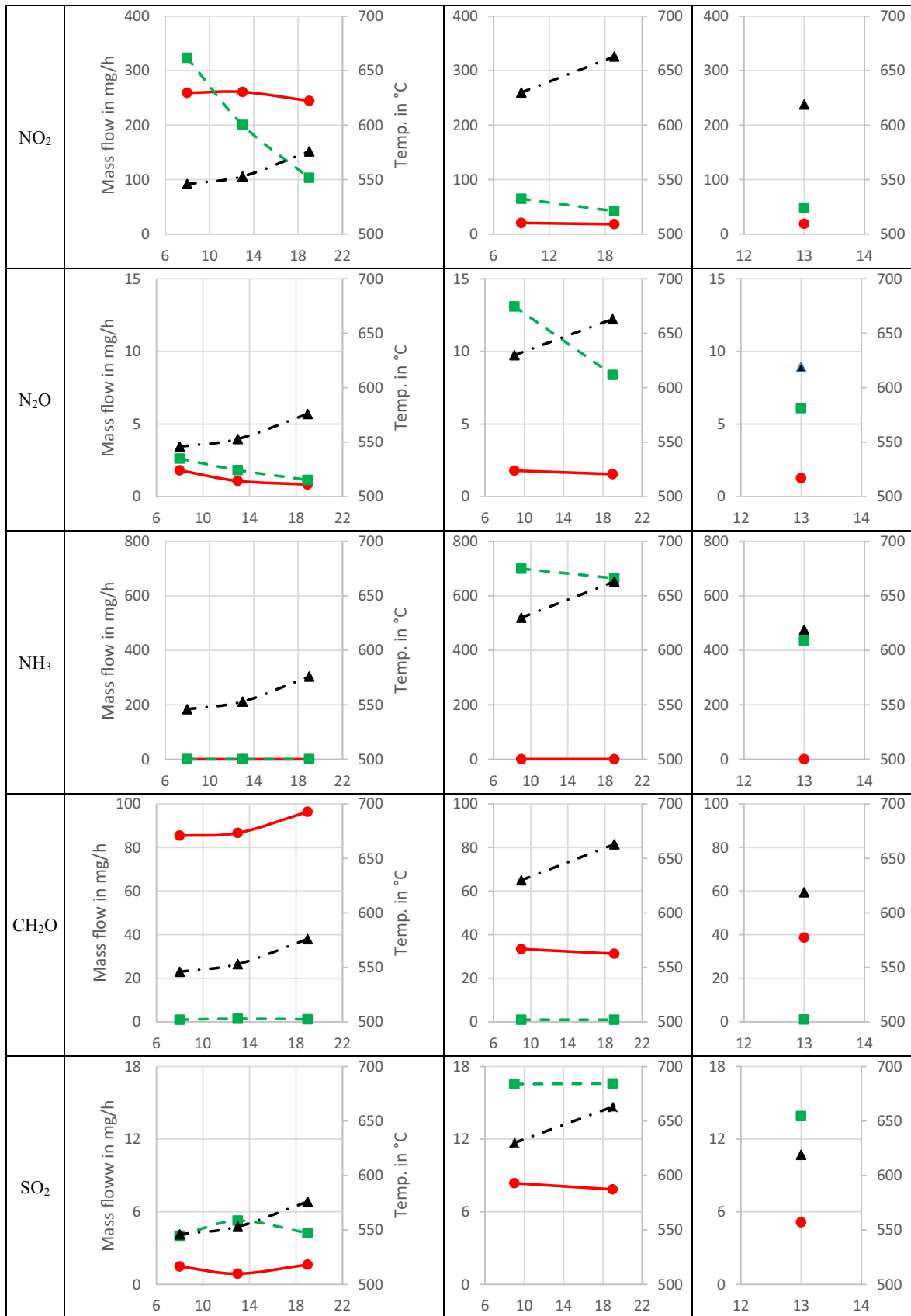
Table 8 (continued)

3.1.4.1 Methane (CH$_4$) *Lean*: Under lean conditions, a late adjustment of the ignition timing from 50% mass fraction burned (MFB50 = 8°CA to MFB50 = 19°CA) leads to a slight reduction of the CH$_4$ raw emission level and an increase of the exhaust temperature by 30 °C (Table 8). Despite the increasing exhaust temperature, the CH$_4$ conversion rate over the catalyst remains almost constant at approx. 80%.

Stoichiometric: Similar trends are observed under stoichiometric conditions, however with overall higher exhaust temperatures of up to 663 °C, lower raw emissions and a lower CH$_4$ conversion of approx. 70%. The positive impacts of higher temperatures seem to be compensated by the higher water amount at altered ignition timing (except one outlier) and its increasing inhibitory effects [24, 25]. Gremminger et al. reported that Pd-based catalysts are most active in lean exhausts, whereas they exhibit only moderate CH$_4$ conversion in stoichiometric exhausts [28]. Our present findings confirm the results of [28], since the almost 90 °C higher exhaust temperature during stoichiometric engine operation cannot compensate lower catalyst activity.

EGR: Dilution of the air and fuel mixture with EGR (10%) at λ = 1 leads to an only minor increase in raw emissions compared to undiluted operation, but results in a slightly lower exhaust temperature and thus in a slight drop in CH$_4$ conversion.

Raw emissions: Dilution by air or also EGR leads to lower combustion temperatures as well as a higher heat capacity of the gas mixture in the cylinder and thus to overall lower combustion chamber temperatures. Thus, the time window in which conditions prevail that benefit methane oxidation is smaller. In addition, the flame speed is reduced. For these reasons, there is less time for the fuel to burn through and more unburnt methane (quenching effects) enters the exhaust gas than that in undiluted operation. The late adjustment of the ignition timing leads to a higher temperature at the end of the working cycle, which benefits catalytic CH$_4$ oxidation. This temperature effect also was observed by Lehtoranta et al. [44].

Post-catalyst emissions: The excess oxygen in lean operation favours the oxidation of unburnt methane in the catalytic converter but also promotes water inhibition, whereas in rich conditions, various reactions have to compete for the remaining oxygen. Theoretically, there is enough oxygen available, but methane conversion is lower due to lower catalytic activity of Pd-based catalysts [28]. Furthermore, it must be taken into account that sulphur in the exhaust gas has a considerable influence on the quality of the catalysis which will be discussed later [27, 49].

3.1.4.2 Carbon monoxide (CO) *Lean*: During lean operation, only minimal differences are shown with regard to the CO raw emissions with the ignition timing variation (Table 8). With later ignition, the emissions are slightly lower. For both ignition angles, the CO is almost completely eliminated by the catalytic converter.

Stoichiometric: The raw emission level during dithering is significantly higher than that in lean operation. With regard to the ignition timing adjustment, analogous effects are observed for stoichiometric and lean conditions. The CO conversion rate is reduced to slightly more than 70%.

EGR: Using EGR, the CO raw emissions are lower than those in stoichiometric operation without EGR, but still significantly higher than those in lean operation. The conversion rate is also just over 70%.

Raw emissions: In general, CO emissions indicate incomplete combustion, as the flame quenches especially near the wall or there may be a local lack of oxygen as a result of inhomogeneities in the combustion chamber. The retarded adjustment of the ignition timing leads to a longer combustion. Consequently, the temperatures required for combustion of the hydrocarbons in the fuel are also present for longer and under lean conditions there is thus more time for oxidation. Under stoichiometric or rich conditions, there are locally more areas of oxygen deficiency, so that the occurrence of incomplete combustion is more frequent [58].

Post-catalyst emissions: The lack of oxygen in the exhaust gas also leads to an increase in emissions after the catalytic converter, as unburnt hydrocarbons cannot be completely oxidized to CO$_2$ and H$_2$O. It is well known from three-way catalysts that CO is converted well under lean conditions, but its conversion decreases under stoichiometric and rich conditions [20, 59].

3.1.4.3 Nitric oxide (NO) *Lean*: During lean operation, a late adjustment of the ignition timing leads to a reduction in NO raw emissions due to the resulting later combustion and thus lower peak temperatures in the combustion chamber (Table 8). In addition, the late adjustment seems to result in a slight increase of the NO concentration measured after the catalyst sample.

Stoichiometric: Under stoichiometric conditions, slightly more than half of the NO is converted by the catalyst. A later ignition under stoichiometric conditions shows the same effect as in the lean. However, the raw emission level is significantly higher due to the higher combustion temperatures, which means that the emissions after catalyst are even partly higher than the raw emissions under lean conditions.

EGR: The use of EGR leads to a similar raw emission level as in lean conditions, but shows the same conversion rate as without EGR.

Raw emissions: Peak combustion temperatures and excess oxygen play a decisive role in the formation of NO. The latter is also present globally under stoichiometric conditions without EGR due to lambda control and locally with the use of EGR due to incomplete mixing. In general, dilution

increases the heat capacity and therefore lowers the peak temperatures during combustion. A late adjustment of the ignition leads to lower peak pressures and thus also to lower maximum temperatures, which also lowers the emissions. The temperature dependency of the NO formation in engines has been sufficiently researched. The main pathway in the engine context is the Zeldovich mechanism describing the NO formation under high temperatures [8, 58, 71].

Post-catalyst emissions: In lean conditions, no conversion takes place in the catalyst (similar to three-way catalysts [20, 59] due to the lack of reducing agents and the inhibitory effect of oxygen on NO reduction that could be observed on Pd-based methane oxidation catalysts [5]. Under stoichiometric conditions, on the contrary, NO conversion takes place, which can at least reduce the increased NO raw emissions resulting from the enrichment to a similar level as in lean conditions.

3.1.4.4 Nitrogen oxide (NO_2)

Lean: While operating lean at early ignition and thus lower exhaust gas temperatures, NO_2 is formed (Table 8). A late adjustment, however, shows a trend reversal and an increase in the NO_2 conversion rate over the catalyst. The raw emissions show no significant influence of the ignition timing.

Stoichiometric: In contrast to lean conditions, the increase of post-catalyst concentration is significant, but is somewhat smaller with a late adjustment of the ignition.

EGR: The use of EGR shows no difference compared to the measurements under stoichiometric conditions without EGR.

Raw emissions: The level of the NO_2 raw emissions decreases significantly during lean operation and thus shows an opposite behaviour to NO. The excess oxygen in lean combustion favours the oxidation of NO to NO_2, which is why the concentrations are higher than those in stoichiometric engine operation.

Post-catalyst emissions: Although additional NO_2 is produced in the catalytic converter due to NO oxidation also in stoichiometric exhausts, the engine-out NO_2 levels are substantially lower and thus the post-catalyst NO_2 concentrations always remain below those found under lean operation.
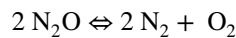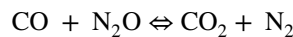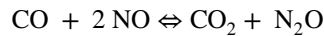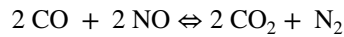
3.1.4.5 Nitrous oxide (N_2O)

Lean: Traces of N_2O (detection limit of the MG 2030 FTIR spectrometer according to the manufacturer at 0.75 ppm) are present especially after the catalytic converter at lean conditions. The late adjustment of the ignition and the associated higher temperatures seem to eliminate the N_2O fractions in the raw exhaust almost completely (Table 8).

Stoichiometric: Compared to lean conditions, the raw emission level is slightly increased and the production rate is significantly higher.

EGR: The use of EGR shows no significant difference to the corresponding operating point without dilution.

Raw emissions: In principle, there are two sources of N_2O: one from combustion in the cylinder and the other from exhaust gas aftertreatment. In the formation of NO in the combustion chamber, the path via N_2O plays an important role in homogeneous charge compression ignition (HCCI) applications [4]. Similar mechanisms could explain the occurrence in the raw exhaust gas. Li et al. observed that incomplete combustion of n-heptane leads to an increase in concentrations in the order of magnitude observed here (approx. 1 ppm) [45].

Post-catalyst emissions: The other source of N_2O emissions are processes in the catalyst. Essentially, the following gross reactions play a role in the conversion, which depend on the catalyst composition, temperature and partial pressure of the individual components:

$$2\,CO\ +\ 2\,NO \Leftrightarrow 2\,CO_2\ +\ N_2$$

$$CO\ +\ 2\,NO \Leftrightarrow CO_2\ +\ N_2O$$

$$CO\ +\ N_2O \Leftrightarrow CO_2\ +\ N_2$$

$$2\,N_2O \Leftrightarrow 2\,N_2\ +\ O_2$$

The first reaction is the desired reduction of NO by CO, and the second describes the undesired formation of N_2O. The decomposition of N_2O with CO acting as a reducing agent is described by the third reaction, and the last one shows a simple dissociation that typically occurs once temperatures exceed 600 °C. It was possible to identify a temperature at which N_2O was no longer formed when syngas was fed to a three-way catalyst (Pd/Rh), independent of the fuel–air mixture, since it dissociates at this temperature. Furthermore, it was shown that only the front zone of the catalyst is important for conversion. N_2O is formed during the incomplete reduction of NO, whereby CO or HC are possible reaction partners. This reaction is favoured in slight excess air, since CO and HC then react first with the atmospheric oxygen. Therefore, fewer CO and HC molecules remain for the reaction with NO than are required for complete reduction. N_2O formation thereby outweighs the degradation mechanisms shown in the fourth reaction at catalyst temperatures of about 200–400 °C [26].

At higher excess air, NO reduction and thus N_2O formation become almost irrelevant. When there is a lack of air, N_2O is formed. At higher temperatures, N_2O reduction with CO or HC dominates [31]. In the study by Adams et al. [1] and Adams et al. [2], the influence of lean-rich alternations on N_2O formation was investigated. It was shown that N_2O was formed mainly in the rich-lean alternations. Moreover,

Gifhorn and Meyer-Pitroff [26] report on a maximum of N_2O formation in slightly lean operation, which is related to the resulting increased NO_x concentration. In the case of the stoichiometric experiments, the lambda oscillation with deflections into richness as well as the increased nitrogen oxide concentrations in the raw exhaust gas due to the higher combustion temperatures could thus have a reinforcing effect on the N_2O formation in the catalytic converter. Significant leaning is shown to be a preventive measure. Despite the higher exhaust gas temperatures compared to 400 °C discussed by Gifhorn and Meyer-Pitroff [26], such eventually existing maximum temperature permitted for formation over the Pd/Al_2O_3 catalyst sample investigated in this publication may not be reached. Furthermore, the presence of sulphur and water leads to deactivation of Pd/Al_2O_3 catalysts with regard to N_2O conversion. [56] In the case of Pt/Al_2O_3 or Pt/SiO_2, N_2O formation is enhanced by water in the feed gas [10]. Both aforementioned effects of sulphur and water, in combination with relatively high NO raw emissions in both lean and stoichiometric conditions, may lead to conditions that favour N_2O-forming reaction pathways. Under stoichiometric (oscillating) conditions, this effect may be further intensified by additional CO raw emissions.

3.1.4.6 Ammonia (NH_3)

Lean: Under lean conditions, ammonia plays a role neither in raw nor post-catalyst emissions. (Table 8).

Stoichiometric: In contrast, catalyst-induced ammonia formation is observed under stoichiometric conditions. Notably, a late adjustment of the ignition timing in the exhaust gas leads to a decrease in ammonia formation.

EGR: In addition, EGR results in reduced ammonia formation in the catalytic converter compared to the pure stoichiometric point without EGR.

Raw emissions: Ammonia plays no role in the raw emissions.

Post-catalyst emissions: If H_2 and NO are present in a certain ratio, ammonia is formed in precious metal catalysts according to the following reaction equation [1]:

$$NO + 5/2\,H_2 \rightarrow NH_3 + H_2O$$
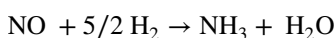
The reaction equation above underscores that in addition to NO, which is often contained in the exhaust gas, the presence of hydrogen is also necessary for ammonia formation. Hydrogen originates from the water contained in the exhaust gas, which reacts with CO according to the so-called water–gas shift reaction (WGS) [1]:

$$CO + H_2O \rightarrow CO_2 + H_2$$
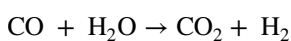
In another study, a positive influence of the modification of Pd/Al_2O_3 with cerium on ammonia formation was observed when H_2O serves as the H_2 source, as this stimulates the water–gas shift. The addition of barium instead of cerium, on the contrary, shows no influence [2]. Note that NH_3 forms only during rich phases when H_2 evolving from WGS is not oxidized due to the lack of oxygen. Furthermore, in these phases, more nitrogen oxides, carbon monoxide as well as water are available as required species. In this regard, the lower ammonia formation in the case of a late adjustment of the ignition may be explained by the lower NO_x content in the raw emissions.

3.1.4.7 Formaldehyde (CH_2O)

Lean: At lean conditions, there is almost no influence of the ignition timing adjustment on the formaldehyde raw emission level (Table 8). The emissions under stoichiometric operation are almost completely converted by the catalyst.

Stoichiometric: Compared to lean conditions, this results in a lower raw emission level, but barely impacts the conversion in the catalyst.

EGR: The use of EGR results in lower raw emissions than those in lean and is about the same level as in undiluted stoichiometric operation.

Raw emissions: Formaldehyde is an intermediate product in methane oxidation, hence its occurrence in exhaust gas suggests incomplete combustion [12, 51]. Consequently, increased formaldehyde emissions always occur along with increased methane emissions and thus the interpretations for raw methane emissions with regard to the influence of dilution by EGR as well as by air also apply in the case of formaldehyde.

Post-catalyst emissions: Regardless of the operating conditions, the Pd/Al_2O_3 catalyst used herein shows an almost complete conversion of the formaldehyde. In the study by Gremminger et al. [28], various noble metal-based catalyst formulations including Pd-based samples were examined for their ability to oxidize formaldehyde under different (simulated) engine-operating conditions. Irrespective of the catalyst composition, almost complete CH_2O conversion was found for temperatures of 350 °C and above. Since all measurements carried out in the present study are well above this temperature, high formaldehyde conversion rates are achieved. However, despite the high catalytic activity, few ppm of CH_2O were detected post-catalyst for all conditions tested, which we attribute to the strong transport limitation of formaldehyde oxidation over noble metal catalysts [70, 73].

3.1.4.8 Sulphur dioxide (SO_2)

In the engine context, SO_2 is the product of combustion of sulphur-containing media that enter the combustion chamber. Gas engines that rely on natural gas or biogas as fuels usually contain sulphur. In the case of natural gas from the city grid, sulphur-containing odorants are added for safety reasons. According to analyses by the Karlsruhe municipal utility, there are

about 5 ppm of sulphur in the natural gas used when it reaches the end consumer. Another source of raw SO_2 emissions can be sulphur-containing engine oil. According to the oil analysis, the SAE40 engine oil used contains 0.14 mass % sulphur. As can be seen in Table 4, the concentrations are max. 4 ppm and thus below or at the detection limit of 4 ppm specified for the FTIR spectrometer used herein for gas analysis, which means that the absolute value should be viewed with caution. However, the pre- and post-catalyst measurements always show the same tendency, so that at least the direction of a change in concentration due to the catalyst could be reliably determined.

Lean: The comparison between the emissions pre- and post-catalyst under lean conditions shows a repeating pattern. The SO_2 level in the raw emissions is always lower than the SO_2 level that is detected at post-catalyst position (Table 8). The exhaust temperatures have no influence on this.

Stoichiometric: Compared to lean conditions, SO_2 is included in the raw emissions at stoichiometry. Emissions after catalyst are also increased. Just as in lean, a late adjustment of the ignition causes no change in the emissions.

EGR: A minor influence with the addition of EGR is seen in the raw emissions, where the proportion is between the stoichiometrically undiluted and the lean in terms of amount.

Raw emissions: Two possible sources play a role in SO_2 formation in the combustion chamber. However, neither seems to play a role in lean-burn, whereas SO_2 is present in the measurements under stoichiometric conditions. The difference between the two operating modes lies in the charging and thus the pressure in the cylinder. To realize the lean conditions, more air must be added with the help of boost pressure while maintaining the load. The cycle thus starts at a higher pressure level than that in uncharged operation during the stoichiometric measurements. When analysing the cylinder pressure curves, it was noticed that at the stoichiometric operating points the pressure is at times below ambient pressure, which sucks oil into the cylinder and therefore results in SO_2 formation during combustion. Conversely, this also could indicate that odorization of the fuel itself plays an only minor role in SO_2 formation, at least for the conditions subject to the present study.

Post-catalyst emissions: According to the case that sulphation has already taken place, the increase in SO_2 emissions after the catalytic converter under rich conditions could be due to regeneration. In the study by Lott et al. [48], it was observed that SO_2 is desorbed under rich conditions and in the presence of water vapour. The lower increase under lean conditions can possibly also be attributed to

the same effects, only much more inhibited. To clarify this conclusively, experiments could be carried out under rich conditions without falling below the ambient pressure in the cylinder by means of charging. In this way, sulphur could be prevented from entering the exhaust gas through combustion of the engine oil and influencing the catalytic activity. However, the piston ring dynamics and the thickness of the oil film on the wall also play a role in the combustion of engine oil both changing with varying operating conditions. Another reason for the increase could be an oxidation of sulphur species in the catalyst which cannot be quantified by the FTIR.

3.1.5 Summary

For a better assessment of the performance of the catalyst under the real engine conditions given in this publication, the most important findings of the measured exhaust gas species are summarized in the following. With regard to NO, the catalytic converter shows no conversion under lean conditions. Dynamic operation with deflections into rich conditions promotes the formation of NO_2, N_2O and NH_3 in the catalytic converter. In addition, there is insufficient CO and NO conversion. In this case, aftertreatment by means of SCR is necessary to cope with the NOx emissions. In this case, the ammonia emissions, which are actually harmful, could prove useful and be used specifically as a reducing agent and at least a partial substitute for urea injection for SCR aftertreatment (passive SCR). To convert 1 g of NOx, 2 g of AdBlue is required [52], which consists of approx. 32.5% urea (($NH_2)_2CO$) [19, 52]. In a first step, thermolysis produces NH_3 and HNCO, which in a second step—the hydrolysis—reacts with water to form NH_3 and CO_2 [52]. With the rate of 2 g_{AdBlue}/g_{NOx}, this results in a total ammonia requirement of 0.37 g_{NH3}/g_{NOx}, which can almost be covered in the case of the stoichiometric measurements shown in this publication with and without EGR (0.30—0.36 g_{NH3}/g_{NOx}). However, as no NH_3 is formed under the lean conditions and the formation rates in the stoichiometric case are only just sufficient to reduce the currently occurring nitrogen oxides, the ammonia formed by the catalysis cannot substitute urea for lean operation. Furthermore, nitrogen oxide emissions may mitigate water inhibition of Pd-based catalysts under certain conditions. With the formation of HNO_2 by means of NO_2, a removal of hydroxyl groups from the Pd catalyst surface has been reported: Hydroxyl groups reduce methane conversion, whereas HNO_2 promotes conversion [62]. Furthermore, NO in the presence of HNO_2 provides significant protection against SO_2 poisoning [7, 29, 62]. These results can help finding an optimal engine operation strategy with regard to exhaust gas aftertreatment.

3.2 Measurements with spatial resolution

3.2.1 Measurement set-up (SpaciPro)

The sampling technique applied for the present study is based on a lab-scale approach that was described in earlier publications [18, 46]. Minor technical adjustments were made to account for engine test bench-specific requirements. For concentration profiling, a quartz glass capillary (I.D. 500 μm, O.D. 660 μm) was inserted into a monolithic sample (300 CPSI, diameter 2.54 cm, length 3.0 cm) coated with PdO/Al_2O_3 catalyst. A motorized linear stage (Zaber Technologies, T-LSM 100A) allowed precise control of the capillary position. Furthermore, a heated sampling loop with a capacity of 10 ml was installed along with a multi-port valve and a pumping system as schematically illustrated in Fig. 6. With this configuration, small amounts of exhaust gas (approx. 150 ml/min) were sucked from inside a single channel of the catalytic converter, until the loop was completely filled. Subsequently, nitrogen originating from a mass flow controller (MFC, Bronkhorst) is used to inject the gaseous sample into the FTIR analyser (MultiGas 2030, MKS Instruments) with a total flow of 1 l/min.

3.2.2 Test procedure and results

To get a better understanding of the effects that occur as a result of dynamic operation that is believed to enhance the catalytic activity, stoichiometric conditions are first examined without and then with dithering and compared with each other. Note that for the tests with spatial resolution, monolith samples with a cell density of 300 cpsi were used to reduce bias of the experiments by the presence of the capillary in a single channel [33]. This reduction of the cell

Table 9 Operating conditions and catalyst for spatially resolved measurements

Engine	
Speed	1500 1/min
Load/IMEP	200 N•m/12,5 bar
Exhaust gas temp	660 °C
Space velocity (GHSV)	200,000 h^{-1}
Catalyst	
Material	2 wt% PdO/Al$_2$O$_3$
Cell density	300 CPSI

density results in a reduction of the catalytic surface and thus of the activity. Therefore, to at least partially compensate for the aforementioned disadvantages, the operating point was also adjusted to a higher load and consequently higher exhaust gas temperatures (see Table 9), while the dithering parameters remain the same. Five consecutive points (corresponding to five times of filling the sample loop and subsequent release into the FTIR analyser) were measured and averaged at each axial position every 5 mm within the channel, as well as 15 and 30 mm behind the catalyst. After calibration of the measured signals, calculations using the FTIR spectra result in the gas-phase species concentrations being present within the monolithic sample.

The engine-out raw emissions were led through a bypass of the exhaust line (c.f. Figure 2) to mimic real-world application parameters such as the temperature and GHSV at the catalyst and simultaneously allow for spatial profiling. Spatially resolved gas-phase species concentrations along the monolithic PdO/Al$_2$O$_3$ catalyst are depicted in Fig. 8. The second highest profile at 60 mm corresponds to a combustion lambda value of 1.4 and an operating load of 30%, which results in an exhaust gas temperature of 530 °C at the inlet and 460 °C at the outlet of the catalyst with a total GHSV
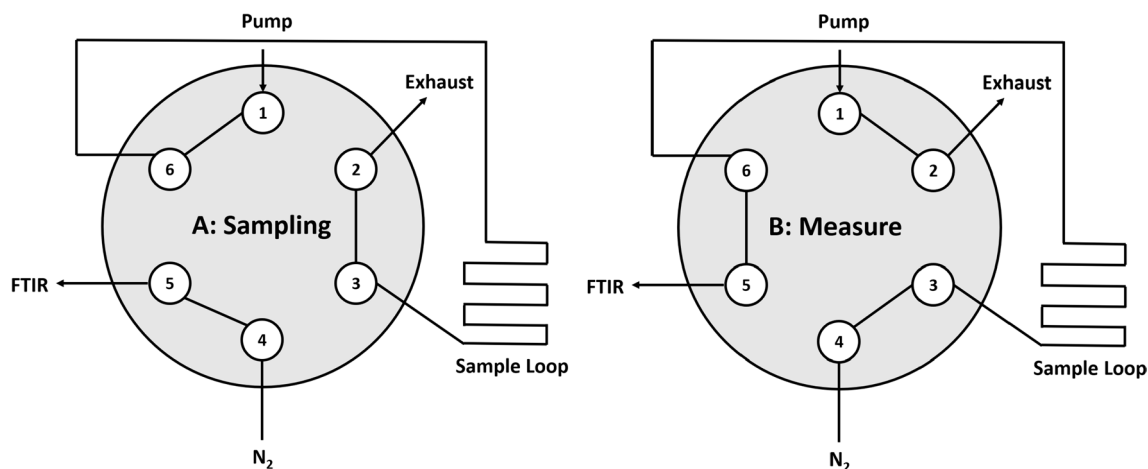

Fig. 6 Principle sketch of the sampling system used for spatially resolved species concentration measurements
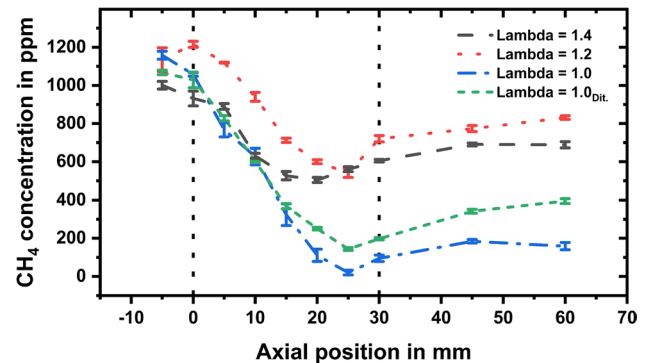
Table 10 Overview of the mean values of certain exhaust gas species

Condition		CH_4 ppm	NO ppm	CO ppm	C_3H_6 ppm	C_3H_8 ppm	O_2 %	H_2O %	T	GHSV 10^5 1/h
Without dithering	Before cat	1256	2653	2305	2.93	14.07	0.53	17.5	668	2.0
	After cat	284	666	214	0.20	1.82	0.02	18.7	587	1.9
	Conversion rate	77%	75%	91%	93%	87%	97%			
With dithering	Before cat	1201	2736	3910	3.34	10.75	0.77	18.5	661	2.0
	After cat	431	1703	1757	1.83	1.74	0.40	18.2	587	1.9
	Conversion rate	64%	38%	55%	45%	84%	49%			
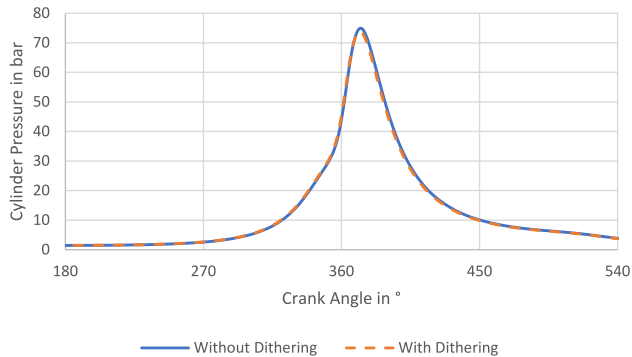
Fig. 7 Comparison of mean cylinder pressure graphs

Fig. 8 CH_4 concentration along catalyst

of 155.000 h^{-1}. With inlet conditions of 13.5% H_2O and around 1050 ppm CH_4, the methane conversion inside the catalytic channel reaches a maximum of 50% after 20 mm. While the CH_4 concentration decreases almost linearly in the front zone of the catalytic channel, the clear maximum in conversion as well as the rise in methane concentration after the monolith can be explained due to the unavoidable interaction between the capillary and the gaseous flow field as discussed in the literature [33]. In conclusion, the low cell density, the moderate exhaust temperature, high water concentrations that inhibit CH_4 activation over the PdO/Al_2O_3 catalyst and a high mass flow result in the overall low CH_4 conversion of around 33%.

Table 10 gives an overview of the most important exhaust gas species and the conversion rates in the Pd-based catalytic converter. It is noticeable that the conversion rates are significantly worse for the measurements in dithering mode. The CH_4 raw emissions are slightly higher without dithering than those with. This could be due to a lower impact of deflections towards rich conditions compared to the ones towards lean conditions where the maximum burn rate of methane is reached and therefore the unburnt methane residues are reduced. The opposite is the case with CO. Here, the low-oxygen operating ranges during dithering seem to have a greater influence on the

raw emissions, so that on average there is almost a doubling compared to the purely stoichiometric mode.

From an engine point of view, the thermodynamic parameters and the influence on engine operation are of particular interest. During a measurement, 200 working cycles are recorded and evaluated. Figure 7 compares the averaged pressure curves of the measurement once with and once without dithering. Only very slight differences in the peak pressure are seen. Another thermodynamic parameter that is used in the engine context to assess the engine smoothness is the coefficient of variation (COV) in relation to the IMEP. The greater the COV, the greater the cyclical fluctuations and thus the smoothness of an engine operation. In this case, the COV of the IMEP increases from 0.6% without dithering to 1.6% with dithering. This can be attributed to the lambda fluctuations, which thereby results in a cyclical change in the cylinder charge composition.

The engine-out raw emissions were led through a bypass of the exhaust line (c.f. Fig. 2) to mimic real-world application parameters such as the temperature and GHSV at the catalyst and simultaneously allow for spatial profiling. Spatially resolved gas-phase species concentrations along the monolithic PdO/Al_2O_3 catalyst are depicted in Fig. 8. The

second highest profile at 60 mm corresponds to a combustion lambda value of 1.4 and an operating load of 30%, which results in an exhaust gas temperature of 530 °C at the inlet and 460 °C at the outlet of the catalyst with a total GHSV of 155.000 h^{-1}. With inlet conditions of 13.5% H_2O and around 1050 ppm CH_4, the methane conversion inside the catalytic channel reaches a maximum of 50% after 20 mm. While the CH_4 concentration decreases almost linearly in the front zone of the catalytic channel, the clear maximum in conversion as well as the rise in methane concentration after the monolith can be explained due to the unavoidable interaction between the capillary and the gaseous flow field as discussed in the literature [33]. In conclusion, the low cell density, the moderate exhaust temperature, high water concentrations that inhibit CH_4 activation over the PdO/Al_2O_3 catalyst and a high mass flow result in the overall low CH_4 conversion of around 33%.

Reducing the lambda value to 1.2 (top profile in Fig. 8) results in an increased exhaust temperature, i.e. 576 °C at the inlet and 490 °C at the outlet of the catalyst, as well as a slightly lower GHSV of 150.000 1/h, which leads to an improved methane conversion. As can be seen in the figure, a maximum CH_4 conversion of 47% is achieved with raw exhaust gas concentration of 1135 ppm CH_4 being emitted by the engine. Technically more species can be monitored with the spatially resolved FTIR measurement; however, for the sake of clarity, only methane emissions are being showed and discussed for the natural gas engine. Due to the lower fuel-to-air ratio, more water is being emitted with a concentration of 16%. Again, the methane concentration declines linearly over the whole length of the monolith channel.

While further decreasing the air-to-fuel ratio to 1.0 and thus stoichiometric conditions, the overall load of the engine was increased to study a different operating point of the engine. As a consequence, not only an increase in space velocity to 195.000 h^{-1} is observed, but also higher exhaust temperatures

of up to 670 °C were achieved at the catalyst that result in higher methane conversion. The engine-out raw emissions of approx. 1160 ppm methane are almost fully oxidized over the PdO/Al_2O_3 catalyst sample. Spatial profiling uncovered a steep decrease of the CH_4 concentration along the catalyst with a maximum CH_4 conversion of 98% after 25 mm. Similar to the other profiles, the CH_4 concentration increased again towards the catalyst outlet (86%) due to the reasons discussed above. Overall, despite the presence of 18% H_2O and the higher space velocity, the higher engine load also leads to an increased exhaust temperature that allows for an improved methane conversion.

Finally, the engine was operated under dithering conditions. Compared to steady stoichiometric engine operation, exhaust temperatures and the GHSV remained essentially constant with values of around 660 °C and 195.000 h^{-1}, respectively. The methane emission however decreased to about 1080 ppm CH_4 on average. As depicted in Fig. 8, the profiles obtained under lambda 1.0 standard operation and dithering strongly resemble and both exhibit a comparably steep almost linear decrease of CH_4.

Note that despite the high water concentrations of up to 19%, the catalyst performance remained mostly stable during the axial profiling experiments at lambda 1.0. Herewith, our results confirm earlier results [6, 13], namely a decreasing relevance of water inhibition at elevated temperatures as present herein (660–670 °C) and at stoichiometric conditions. In addition, dithering conditions can stabilize conversion rates over time because rich conditions [21], even if only applied very shortly, facilitate the desorption of hydroxyl groups from the catalyst surface that would otherwise block active sites [22]. Regarding the stability of the catalyst, a stabilizing effect of the dithering mode is noticeable compared to the static mode where an increase of the post-catalyst emissions can be seen (Fig. 9).

Fig. 9 CH_4 concentrations over measurement time with the higher level of emissions representing the pre catalyst values and the lower level showing the one measured post-catalyst
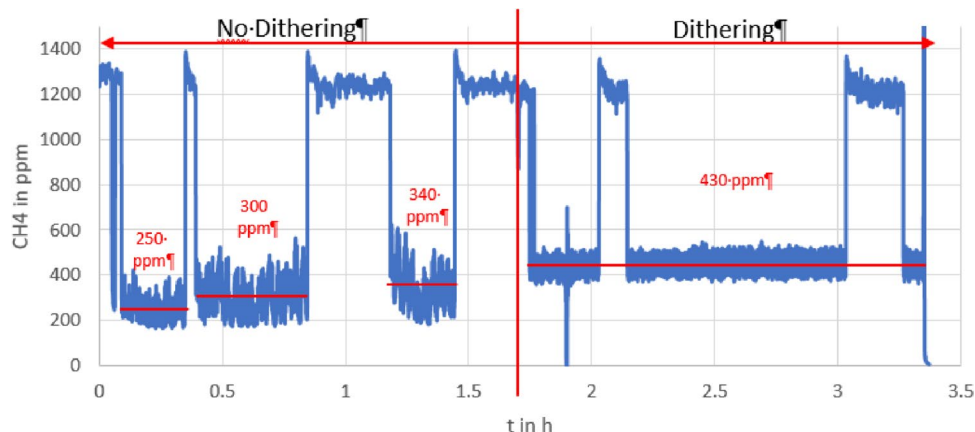
4 Conclusion

To investigate the influence of exhaust gas conditions of lean-burn gas engines on a methane oxidation catalyst (PdO/Al_2O_3), a serial engine that is originally operated under stoichiometric conditions was converted to supercharged operation. It was then coupled with an exhaust system that enables to investigate the impact of real exhaust gas conditions onto a catalyst sample produced on a laboratory scale. This is realized with the help of a bypass line in which the sample can be installed interchangeably. To ensure real conditions at the catalytic converter, a reference location is first defined that would correspond to the installation location of a series catalytic converter. This is usually after the turbocharger. Since no series turbocharger is available in this test set-up, the reference point is defined behind the backpressure valve (simulation of the flow resistance of the turbocharger). A throttle valve is used to control the exhaust gas mass flow and thus the space velocity at the sample so that it corresponds to the one at the reference position. The catalytic converter volume for the reference GHSV calculation equals the volume of the series catalytic converter and thus considers the retrofit idea. Another important parameter is the temperature, which is also controlled to the temperature at the reference point with the help of a heating tape. The quality of the control is shown by the deviation of the setpoint values from the actual values of the space velocities averaged over the operating points which is 0.1% on average across all measurements. Furthermore, a comparison of the pressure conditions at the catalytic converter with those after the engine shows that the pressure pulsation resulting from real engine operation is also passed on to the sample in the bypass line.

With the novel experimental setup, it is now possible to measure detailed exhaust gas compositions under realistic, technically relevant conditions upstream and downstream of the sample using an FTIR spectrometer. This measurement setup is then used to carry out exhaust gas tests during two important operating modes. To simulate exhaust gas boundary conditions as they are found in maritime and stationary applications, lean operation is investigated first and finally compared with stoichiometric operation. Particular focus is laid on dynamic lean-rich cycling, the so-called dithering, to evaluate whether the short rich phases that are known to regenerate deactivated Pd-based methane oxidation catalysts can contribute to high and stable catalyst performance. A random test with an exhaust gas recirculation rate of 10% is considered as well.

With regard to NO, the catalytic converter shows no conversion under lean conditions. In dynamic operation under lean-rich cycling around lambda equal to 1, the formation of NO_2, N_2O and NH_3 in the catalytic converter increases and CO as well as NO conversion is overall low, which is due to the short rich phases. Therefore, aftertreatment by means of SCR is necessary for technical applications to reduce the NO_x emissions. In this case, the formation of ammonia in the Pd-based oxidation catalyst may prove useful as a reducing agent and at least a partial substitute for urea injection for SCR aftertreatment (passive SCR) for stoichiometric conditions. However, as no NH_3 is formed under the lean conditions and the formation rates in the stoichiometric case are only just sufficient to reduce the currently occurring nitrogen oxides, the ammonia formed by the catalysis cannot substitute urea for lean operation. Furthermore, high engine-out nitrogen oxide levels and particularly the formation of NO_2 over the catalyst may help to mitigate water inhibition of CH_4 oxidation over PdO/Al_2O_3. Sulphur species that poison Pd-based catalysts were found to originate from the fuel itself as well as from engine oil, with the latter being particularly critical as comparably high sulphur levels can occur at least temporarily. Overall, the CH_4 conversion over the PdO/Al_2O_3 catalyst was higher under lean conditions than that in stoichiometric operation. Dynamic lean-rich cycling around lambda = 1, the so-called dithering, stabilizes the catalytic activity and prevents the well-known deactivation of Pd-based catalysts induced by water. The beneficial effect of dithering is attributed to the short rich phases that facilitate the desorption of hydroxyl groups that would otherwise block active sites.

In addition to raw exhaust gas analysis and end of pipe measurements, the exhaust gas composition was analysed within a single catalyst channel using a capillary technique designed for obtaining spatially resolved gas-phase species concentration profiles. The profiles uncovered an almost linear decrease of the CH_4 conversion along a single catalyst channel for all conditions tested. Switching from leaner to richer engine operation modes clearly influenced the catalytic activity, which can be attributed to the complex interaction of exhaust gas temperature, space velocity and species concentrations. The coupling of a full-scale engine test bench with the SpaciPro technique for investigating catalyst samples with spatial resolution allows to deconvolute the various phenomena taking place on the catalyst simultaneously in realistic exhaust gases. Future investigations will therefore allow to harmonize engine control strategies with catalyst operation modes to minimize the emissions from gas engines.

Appendix

See Table 11.

Table 11 Overview of the used measurement devices

	Analyser	Measuring principle	Manufacturer	Measuring location/measuring medium
Gas composition	IRD CO2/COh	Non-dispersive infrared analyser CO_2/CO high	AVL	Raw exhaust gas and after catalyst
	PMD O2	Paramagnetic O2 analyser	AVL	Raw exhaust gas and after catalyst
	IRD 4000 COl	Non-dispersive infrared analyser CO low	AVL	Raw exhaust gas and after catalyst
	CLD 4000 hhd	Chemiluminescence detector undiluted, hot measurement	AVL	Raw exhaust gas and after catalyst
	Cutter FID I60 LHD	Flame ionization detector diluted, hot measurement	AVL	Raw exhaust gas and after catalyst
	FTIR	Fourier transform infrared spectrometer	IAG	Raw exhaust gas and after catalyst
	Lambda-Meter	Lambda	ETAS	Raw exhaust gas
	Lambda-Sensor LSU4.9	Lambda	Bosch	Raw exhaust gas
	URAS	Non-dispersive infrared analyser	ABB	CO_2 composition at inlet and exhaust
	TOTALFLOW	Gas chromatograph	ABB	Natural gas
	AFK-G	Humidity	Kobold	Charge air
Pressure indication	6056AU20	High pressure relative	Kistler	Cylinder 1
	6056AU20	High pressure relative	Kistler	Cylinder 2
	6056AU20	High pressure relative	Kistler	cylinder 3
	4075A10V39	Low pressure absolute	Kistler	Intake manifold
	4049A5S	Low pressure absolute	Kistler	Exhaust gas after engine
	4075A10V200S	Low pressure absolute	Kistler	Exhaust gas before catalyst
	4045A5	Low pressure absolute	Kistler	Exhaust gas after catalyst
Flow measurement	EcoRPM	Volume flow via rotary piston gas metre (rotary piston metre)	RMA	Charge air
	PROMASS 83	Mass flow via Coriolis	Endress + Hauser	Natural gas
	DF8	Mass flow via differential pressure transmitter	Systec	Exhaust gas in bypass

Declarations

Conflict of interest The authors declare that they have no known competing financial interests or personal relationships that could have appeared to influence the work reported in this paper.

References

1. Adams, E.C., Skoglundh, M., Folic, M., Bendixen, E.C., Gabrielsson, P., Carlsson, P.-A.: Ammonia formation over supported platinum and palladium catalysts. Appl. Catal. B **165**, 10–19 (2015). https://doi.org/10.1016/j.apcatb.2014.09.064

2. Adams, E.C., Skoglundh, M., Gabrielsson, P., Laurell, M., Carlsson, P.-A.: Ammonia formation over Pd/Al2O3 modified with cerium and barium. Catalysis Today **267**, 210–216 (2016). https://doi.org/10.1016/j.cattod.2016.01.012

3. Alyani, M., Smith, K.J.: Kinetic analysis of the inhibition of CH 4 oxidation by H2O on PdO/Al2O3 and CeO2/PdO/Al2O3 catalysts. Ind. Eng. Chem. Res. **55**(30), 8309–8318 (2016). https://doi.org/10.1021/acs.iecr.6b01881

4. Amnéus, P., Mauss, F., Kraft, M., Vressner, A., Johansson, B.: NOx and N2O formation in HCCI engines. In: SAE Technical Paper 2005-01-0126 (2005). https://doi.org/10.4271/2005-01-0126

5. Andersson, B., Cruise, N., Lunden, M., Hansson, M.: Methane and nitric oxide conversion over a catalyst dedicated for natural gas vehicles. In: SAE Technical Paper Series. International Fuels & Lubricants Meeting & Exposition, OCT. 16, 2000. SAE Technical Paper Series. SAE International400 Commonwealth Drive, Warrendale, PA, United States (2000). https://doi.org/10.4271/2000-01-2928

6. Arosio, F., Colussi, S., Trovarelli, A., Groppi, G.: Effect of alternate CH4-reducing/lean combustion treatments on the reactivity of fresh and S-poisoned Pd/CeO2/Al2O3 catalysts. Appl. Catal. B Environ. **80**(3–4), 335–342 (2008). https://doi.org/10.1016/j.apcatb.2007.11.030

7. Auvinen, P., Kinnunen, N.M., Hirvi, J.T., Maunula, T., Kallinen, K., Keenan, M., Suvanto, M.: Effects of NO and NO2 on fresh and SO2 poisoned methane oxidation catalyst—harmful or beneficial? Chem. Eng. J. **417**(128050), 1385–8947 (2021). https://doi.org/10.1016/j.cej.2020.128050

8. Baulch, D.L., Cobos, C.J., Cox, R.A., Frank, P., Hayman, G., Just, T., Kerr, J.A., Murrells, T., Pilling, M.J., Troe, J., Walker, R.W., Warnatz, J.: Evaluated kinetic data for combustion modeling. Suppl. I J. Phys. Chem. Refer. Data **23**(6), 847–848 (1994). https://doi.org/10.1063/1.555953

9. Bounechada, D., Groppi, G., Forzatti, P., Kallinen, K., Kinnunen, T.: Effect of periodic lean/rich switch on methane conversion over a Ce–Zr promoted Pd-Rh/Al2O3 catalyst in the exhausts of natural gas vehicles. Appl. Catal. B Environ. **119–120**, 91–99 (2012). https://doi.org/10.1016/j.apcatb.2012.02.025

10. Burch, R.: An investigation of the NO/H2/O2 reaction on noble-metal catalysts at low temperatures under lean-burn conditions. Appl. Catal. B Environ. **23**(2–3), 115–121 (1999). https://doi.org/10.1016/S0926-3373(99)00073-9

11. Castellazzi, P., Groppi, G., Forzatti, P.: Effect of Pt/Pd ratio on catalytic activity and redox behavior of bimetallic Pt–Pd/Al2O3 catalysts for CH4 combustion. Appl. Catal. B Environ. **95**(3–4), 303–311 (2010). https://doi.org/10.1016/j.apcatb.2010.01.008

12. CIMAC WG17: Methane and formaldehyde emissions of gas engines (2014)

13. Ciuparu, D., Pfefferle, L.: Methane combustion activity of supported palladium catalysts after partial reduction. Appl. Catal. A **218**(1–2), 197–209 (2001). https://doi.org/10.1016/S0926-860x(01)00643-3

14. Ciuparu, D., Lyubovsky, M.R., Altman, E., Pfefferle, L.D., Datye, A.: Catalytic combustion of methane over palladium-based catalysts. Catal. Rev. **44**(4), 593–649 (2002). https://doi.org/10.1081/CR-120015482

15. Ciuparu, D., Bozon-Verduraz, F., Pfefferle, L.: Oxygen exchange between palladium and oxide supports in combustion catalysts. J. Phys. Chem. B **106**(13), 3434–3442 (2002). https://doi.org/10.1021/jp013577r

16. Ciuparu, D., Perkins, E., Pfefferle, L.: In situ DR-FTIR investigation of surface hydroxyls on γ-Al2O3 supported PdO catalysts during methane combustion. Appl. Catal. A Gen. **263**(2), 145–153 (2004). https://doi.org/10.1016/j.apcata.2003.12.006

17. Deka, D.J., Pihl, J.A., Thomas, C.R., Partridge, W.P.: Intra-catalyst CH4 oxidation pathways on a Pd/Al2O3/CeZrOx-based commercial catalyst and implications on NOx conversion profiles for a natural gas vehicle exhaust under lambda modulation. Chem. Eng. J. **472**(144803), 1385–8947 (2023). https://doi.org/10.1016/j.cej.2023.144803

18. Diehm, C., Karadeniz, H., Karakaya, C., Hettel, M., Deutschmann, O.: Spatial resolution of species and temperature profiles in catalytic reactors. Adv. Chem. Eng. **45**, 41–95 (2014). https://doi.org/10.1016/B978-0-12-800422-7.00002-9

19. DIN Deutsches Institut für Normung e.V.: DIN 70070 - Diesel engines—NOx-Reduction agent AUS 32—quality requirements. Beuth Verlag GmbH, 10772 Berlin

20. Farrauto, R.J., Heck, R.M.: Catalytic converters: state of the art and perspectives. Catal. Today **51**(3–4), 351–360 (1999). https://doi.org/10.1016/S0920-5861(99)00024-3

21. Ferri, D., Elsener, M., Kröcher, O.: Methane oxidation over a honeycomb Pd-only three-way catalyst under static and periodic operation. Appl. Catal. B **220**, 67–77 (2018). https://doi.org/10.1016/j.apcatb.2017.07.070

22. Franken, T., Roger, M., Petrov, A.W., Clark, A.H., Agote-Arán, M., Krumeich, F., Kröcher, O., Ferri, D.: Effect of short reducing pulses on the dynamic structure, activity, and stability of Pd/Al2O3 for wet lean methane oxidation. ACS Catal. **11**(8), 4870–4879 (2021). https://doi.org/10.1021/acscatal.1c00328

23. Gélin, P., Primet, M.: Complete oxidation of methane at low temperature over noble metal based catalysts: a review. Appl. Catal. B **39**(1), 1–37 (2002). https://doi.org/10.1016/S0926-3373(02)00076-0

24. Gélin, P., Urfels, L., Primet, M., Tena, E.: Complete oxidation of methane at low temperature over Pt and Pd catalysts for the abatement of lean-burn natural gas fuelled vehicles emissions: influence of water and sulphur containing compounds. Catal. Today **83**(1–4), 45–57 (2003). https://doi.org/10.1016/S0920-5861(03)00215-3

25. Gholami, R., Alyani, M., Smith, K.: Deactivation of Pd catalysts by water during low temperature methane oxidation relevant to natural gas vehicle converters. Catalysts **5**(2), 561–594 (2015). https://doi.org/10.3390/catal5020561

26. Gifhorn, A., Meyer-Pitroff, R.: Einfluß abgasspezifischer Parameter auf die N2O-Bildung am Pd/Rh-Katalysator. MTZ Motortech Z **59**(6), 378–383 (1998). https://doi.org/10.1007/BF03226460

27. Gremminger, A., Lott, P., Merts, M., Casapu, M., Grunwaldt, J.-D., Deutschmann, O.: Sulfur poisoning and regeneration of bimetallic Pd-Pt methane oxidation catalysts. Appl. Catal. B **218**, 833–843 (2017). https://doi.org/10.1016/j.apcatb.2017.06.048

28. Gremminger, A., Pihl, J., Casapu, M., Grunwaldt, J.-D., Toops, T.J., Deutschmann, O.: PGM based catalysts for exhaust-gas aftertreatment under typical diesel, gasoline and gas engine conditions with focus on methane and formaldehyde oxidation. Appl. Catal. B Environ. **265**, 118571 (2020). https://doi.org/10.1016/j.apcatb.2019.118571

29. Gremminger, A.T., Pereira de Carvalho, H.W., Popescu, R., Grunwaldt, J.-D., Deutschmann, O.: Influence of gas composition on activity and durability of bimetallic Pd-Pt/Al2O3 catalysts for total oxidation of methane. Catalysis Today **258**, 470–480 (2015). https://doi.org/10.1016/j.cattod.2015.01.034

30. Hansen, T.W., Delariva, A.T., Challa, S.R., Datye, A.K.: Sintering of catalytic nanoparticles: particle migration or Ostwald ripening? Acc. Chem. Res. **46**(8), 1720–1730 (2013). https://doi.org/10.1021/ar3002427

31. Hausberger, S.: N2O aus mobilen Quellen ACCC-Workshop "N2O und das Kyoto-Ziel" (1999)

32. Hegedus, L.L., Chang, C.C., McEwen, D.J., Sloan, E.M.: Response of catalyst surface concentrations to forced concentration oscillations in the gas phase. The NO, CO, O2 system over Pt-alumina. Ind. Eng. Chem. Fund. **19**(4), 367–373 (1980). https://doi.org/10.1021/i160076a008

33. Hettel, M., Diehm, C., Torkashvand, B., Deutschmann, O.: Critical evaluation of in situ probe techniques for catalytic honeycomb monoliths. Catal. Today **216**, 2–10 (2013). https://doi.org/10.1016/j.cattod.2013.05.005

34. Hodonj, D., Borchers, M., Zeh, L., Hoang, G.T., Tischer, S., Lott, P., Deutschmann, O.: Impact of operation parameters and lambda input signal during lambda-dithering of three-way catalysts for low-temperature performance enhancement. Appl. Catal. B **345**, 123657 (2024). https://doi.org/10.1016/j.apcatb.2023.123657

35. Howarth, R.W.: A bridge to nowhere: methane emissions and the greenhouse gas footprint of natural gas. Energy Sci. Eng. **2**(2), 47–60 (2014). https://doi.org/10.1002/ese3.35

36. Hurtado, P., Ordonez, S., Sastre, H., Diez, F.V.: Development of a kinetic model for the oxidation of methane over Pd/Al2O3 at dry and wet conditions. Appl. Catal. B Environ. **51**(4), 229–238 (2004). https://doi.org/10.1016/j.apcatb.2004.03.006

37. Karinshak, K.A., Lott, P., Harold, M.P., Deutschmann, O.: In situ activation of bimetallic Pd−Pt methane oxidation catalysts. ChemCatChem **12**(14), 3712–3720 (2020). https://doi.org/10.1002/cctc.202000603

38. Keller, K., Lott, P., Stotz, H., Maier, L., Deutschmann, O.: Microkinetic modeling of the oxidation of methane over PdO catalysts—towards a better understanding of the water inhibition effect. Catalysts **10**(8), 922 (2020). https://doi.org/10.3390/catal10080922

39. Keller, K., Lott, P., Tischer, S., Casapu, M., Grunwaldt, J.-D., Deutschmann, O.: Methane oxidation over PdO: towards a better understanding of the influence of the support material. ChemCatChem **15**(11) (2023). https://doi.org/10.1002/cctc.202300366

40. Koberstein, H., Meyer, R., Niedermeier, N., Zajonz, M.: Wie es um unsere Gasversorgung steht. https://www.zdf.de/nachrichten/wirtschaft/gasversorgung-energiesicherheit-deutschland-pipelines-russland-100.html (2023). Accessed 3 November 2023

41. Krivopolianskii, V., Valberg, I., Stenersen, D., Ushakov, S., Æsøy, V.: Control of the combustion process and emission formation in marine gas engines. J. Mar. Sci. Technol. **24**(2), 593–611 (2019). https://doi.org/10.1007/s00773-018-0556-0

42. Lapisardi, G., Urfels, L., Gélin, P., Primet, M., Kaddouri, A., Garbowski, E., Toppi, S., Tena, E.: Superior catalytic behaviour of Pt-doped Pd catalysts in the complete oxidation of methane at low temperature. Catal. Today **117**(4), 564–568 (2006). https://doi.org/10.1016/j.cattod.2006.06.004

43. Lee, J., Lim, T.H., Lee, E., Kim, D.H.: Promoting the methane oxidation on Pd/CeO2 catalyst by increasing the surface oxygen mobility via defect engineering. ChemCatChem **13**(16), 3706–3712 (2021). https://doi.org/10.1002/cctc.202100653

44. Lehtoranta, K., Koponen, P., Vesala, H., Kallinen, K., Maunula, T.: Performance and regeneration of methane oxidation catalyst for LNG ships. JMSE **9**(2), 111 (2021). https://doi.org/10.3390/jmse9020111

45. Li, H., Neill, W.S., Guo, H., Chippior, W.: The NOx and N2O emission characteristics of an HCCI engine operated with n-Heptane. J. Energy Resour. Technol **134**(1) (2012). https://doi.org/10.1115/1.4005243

46. Livio, D., Diehm, C., Donazzi, A., Beretta, A., Deutschmann, O.: Catalytic partial oxidation of ethanol over Rh/Al2O3: Spatially resolved temperature and concentration profiles. Appl. Catal. A Gen. **467**, 530–541 (2013). https://doi.org/10.1016/j.apcata.2013.07.054

47. Lott, P., Eck, M., Doronkin, D.E., Popescu, R., Casapu, M., Grunwaldt, J.-D., Deutschmann, O.: Regeneration of sulfur poisoned Pd–Pt/CeO2–ZrO2-Y2O3–La2O3 and Pd–Pt/Al2O3 methane oxidation catalysts. Top Catal. **62**(1–4), 164–171 (2019). https://doi.org/10.1007/s11244-018-1121-0

48. Lott, P., Eck, M., Doronkin, D.E., Zimina, A., Tischer, S., Popescu, R., Belin, S., Briois, V., Casapu, M., Grunwaldt, J.-D., Deutschmann, O.: Understanding sulfur poisoning of bimetallic Pd-Pt methane oxidation catalysts and their regeneration. Appl. Catal. B **278**, 119244 (2020). https://doi.org/10.1016/j.apcatb.2020.119244

49. Lott, P., Casapu, M., Grunwaldt, J.-D., Deutschmann, O.: A review on exhaust gas after-treatment of lean-burn natural gas engines—from fundamentals to application. Appl. Catal. B Environ. **340**, 123241 (2024). https://doi.org/10.1016/j.apcatb.2023.123241

50. Maersk Mc-Kinney Moller Center: Reducing methane emissions onboard vessels: an overview of methane emission sources and levels onboard vessels and the technologies, solutions, and regulatory drivers that can help reduce them (2022)

51. Mitchell, C.E., Olsen, D.B.: Formaldehyde formation in large bore natural gas engines part 1: formation mechanisms. J. Eng. Gas Turbines Power **122**(4), 603–610 (2000). https://doi.org/10.1115/1.1290585

52. Mollenhauer, K. (ed): Handbuch Dieselmotoren: Mit 84 Tabellen, 3rd edn. VDI. Springer, Berlin(2007)

53. Muraki, H., Fujitani, Y.: Nitric oxide reduction by carbon monoxide over noble-metal catalysts under cycled feedstreams. Ind. Eng. Chem. Prod. Res. Dev. **25**(3), 414–419 (1986). https://doi.org/10.1021/i300023a008

54. Murata, K., Kosuge, D., Ohyama, J., Mahara, Y., Yamamoto, Y., Arai, S., Satsuma, A.: Exploiting metal–support interactions to tune the redox properties of supported Pd catalysts for methane combustion. ACS Catal. **10**(2), 1381–1387 (2020). https://doi.org/10.1021/acscatal.9b04524

55. Narui, K., Yata, H., Furuta, K., Nishida, A., Kohtoku, Y., Matsuzaki, T.: Effects of addition of Pt to PdO/Al2O3 catalyst on catalytic activity for methane combustion and TEM observations of supported particles. Appl. Catal. A Gen. **179**(1–2), 165–173 (1999). https://doi.org/10.1016/S0926-860X(98)00306-8

56. Pekridis, G., Athanasiou, C., Konsolakis, M., Yentekakis, I.V., Marnellos, G.E.: N2O Abatement over γ-Al2O3 supported catalysts: effect of reducing agent and active phase nature. Top Catal. **52**(13–20), 1880–1887 (2009). https://doi.org/10.1007/s11244-009-9346-6

57. Persson, K., Pfefferle, L.D., Schwartz, W., Ersson, A., Järås, S.G.: Stability of palladium-based catalysts during catalytic combustion of methane: the influence of water. Appl. Catal. B **74**(3–4), 242–250 (2007). https://doi.org/10.1016/j.apcatb.2007.02.015

58. Pischinger, R., Klell, M., Sams, T.: Thermodynamik der Verbrennungskraftmaschine, 3rd edn. Der Fahrzeugantrieb. Springer Vienna; Imprint: Springer, Vienna (2009)

59. Raj, B.A.: Methane emission control Johnson Matthey. Technol. Rev. **60**(4), 228–235 (2016). https://doi.org/10.1595/205651316X692554

60. Roger, M., Kröcher, O., Ferri, D.: Assessing the effect of O2 dithering on CH4 oxidation on Pd/Al2O3 1385-8947. Chem. Eng. J. **451**, 138865 (2023). https://doi.org/10.1016/j.cej.2022.138865

61. Sá, J., Fernandes, D.L.A., Aiouache, F., Goguet, A., Hardacre, C., Lundie, D., Naeem, W., Partridge, W.P., Stere, C.: SpaciMS: spatial and temporal operando resolution of reactions within catalytic monoliths. The Analyst **135**(9), 2260–2272 (2010). https://doi.org/10.1039/c0an00303d

62. Sadokhina, N., Smedler, G., Nylén, U., Olofsson, M., Olsson, L.: The influence of gas composition on Pd-based catalyst activity in methane oxidation—inhibition and promotion by NO. Appl. Catal. B Environ. **200**, 351–360 (2017). https://doi.org/10.1016/j.apcatb.2016.07.012

63. Shi, X., Seiser, R., Chen, J.-Y., Dibble, R., Cattolica, R.: Fuel-dithering optimization of efficiency of TWC on natural gas IC engine SAE. Int. J. Engines **8**(3), 1246–1252 (2015). https://doi.org/10.4271/2015-01-1043

64. Stotz, H., Maier, L., Boubnov, A., Gremminger, A.T., Grunwaldt, J.-D., Deutschmann, O.: Surface reaction kinetics of methane oxidation over PdO. J. Catal. **370**, 152–175 (2019). https://doi.org/10.1016/j.jcat.2018.12.007

65. Talei, M., Jafarmadar, S., Khalilarya, S.: Experimental and numerical analyses of cold EGR effect on combustion, performance and emissions of natural gas lean-burn engine with pre-chamber combustion system. Fuel **276**, 118061 (2020). https://doi.org/10.1016/j.fuel.2020.118061

66. Tavakoli, S., Schramm, J., Pedersen, E.: Strategies on methane slip mitigation of spark-ignition natural gas engine during transient motion. SAE Int. (2021). https://doi.org/10.4271/2021-01-5062

67. Verbrennung, T.: Verbrennungstechnik, Verbrennungsmodellierung, Emissionen. Springer-Verlag, Berlin (2006)

68. Tomin, S., Wagner, U., Koch, T.: Influence of real CNG engine emissions On PdO/Al2O3 methane oxidation catalysts engineering. Today Open Access J. **5(4)** (2023). https://doi.org/10.19080/ETOAJ.2023.05.555669

69. Tomin, S., Wagner, U., and Koch, T.: Effect of Dithering on post-catalyst exhaust gas composition and on short time regeneration of deactivated PdO/Al2O3 catalysts under real engine conditions, SAE Technical Paper 2024-37-0002, (2024). **(in press)**

70. Torkashvand, B., Maier, L., Hettel, M., Schedlbauer, T., Grunwaldt, J.-D., Deutschmann, O.: On the challenges and constrains of ultra-low emission limits: formaldehyde oxidation in catalytic sinusoidal-shaped channels. Chem. Eng. Sci. **195**, 841–850 (2019). https://doi.org/10.1016/j.ces.2018.10.031

71. van Basshuysen, R.: Erdgas und erneuerbares Methan für den Fahrzeugantrieb. Springer Fachmedien Wiesbaden, Wiesbaden (2015)

72. Velin, P., Hemmingsson, F., Schaefer, A., Skoglundh, M., Lomachenko, K.A., Raj, A., Thompsett, D., Smedler, G., Carlsson, P.-A.: Hampered PdO redox dynamics by water suppresses lean methane oxidation over realistic palladium catalysts. ChemCatChem **13**(17), 3765–3771 (2021). https://doi.org/10.1002/cctc.202100829

73. Wan, S., Torkashvand, B., Häber, T., Suntz, R., Deutschmann, O.: Investigation of HCHO catalytic oxidation over platinum using planar laser-induced fluorescence. Appl. Catal. B **264**, 118473 (2020). https://doi.org/10.1016/j.apcatb.2019.118473

74. Wang, Gong, J., Luo, J., Li, J., Kamasamudram, K., Currier, N., Yezerets, A.: Distinct reaction pathways of methane oxidation on different oxidation states over Pd-based three-way catalyst (TWC). Appl. Catal. A Gen. **572**, 44–50 (2019). https://doi.org/10.1016/j.apcata.2018.12.022

75. Wildes, H., Fridell, E., Ellis, J., Forsman, B., Ramsay, W., Westermark, H.: Aftertreatment of methane slip from marine gas engines: an overview of the issue in a context of emission levels, engine trends and sustainability matters, including a case study involving installation of a catalyst on a tanker (2020)